

See discussions, stats, and author profiles for this publication at: <https://www.researchgate.net/publication/265131034>

# A generalized equilibrium model for predicting daily to inter-annual shoreline response

Article in *Journal of Geophysical Research: Earth Surface* · September 2014

Impact Factor: 3.44 · DOI: 10.1002/2014JF003106

CITATIONS

13

READS

163

6 authors, including:



[Kristen Splinter](#)

University of New South Wales

49 PUBLICATIONS 225 CITATIONS

SEE PROFILE



[Ian L Turner](#)

University of New South Wales

152 PUBLICATIONS 2,770 CITATIONS

SEE PROFILE



[Mark A Davidson](#)

University of Plymouth

98 PUBLICATIONS 1,225 CITATIONS

SEE PROFILE



[Patrick L. Barnard](#)

United States Geological Survey

93 PUBLICATIONS 1,551 CITATIONS

SEE PROFILE

1 **A generalized equilibrium model for predicting daily**  
2 **to inter-annual shoreline response**

Kristen D. Splinter

3 Water Research Laboratory, School of Civil and Environmental Engineering,  
4 UNSW Australia, Sydney, NSW, Australia

Ian L. Turner

5 Water Research Laboratory, School of Civil and Environmental Engineering,  
6 UNSW Australia, Sydney, NSW, Australia

Mark A. Davidson

7 School of Marine Science and Engineering, University of Plymouth,  
8 Plymouth, Devon, UK

Patrick Barnard

9 United States Geological Survey, Pacific Coastal and Marine Science Center,  
10 400 Natural Bridges Drive, Santa Cruz, CA, USA

Bruno Castelle

11 Universite Bordeaux; CNRS; UMR 5805 EPOC, Avenue des Facultes,  
12 F-33405 Talence, France

Joan Oltman-Shay

13 NorthWest Research Associates, 4118 148th Ave NE, Redmond, WA, USA

14 **Abstract.** Coastal zone management requires the ability to predict coast-  
15 line response to storms and longer-term seasonal to inter-annual variability  
16 in regional wave climate. Shoreline models typically rely on extensive his-  
17 torical observations to derive site-specific calibration. To circumvent the chal-  
18 lenge that suitable data sets are rarely available, this contribution utilizes  
19 twelve 5+ year shoreline data sets from around the world to develop a gen-  
20 eralized model for shoreline response. The shared dependency of model co-  
21 efficients on local wave and sediment characteristics is investigated, enabling  
22 the model to be recast in terms of these more readily measurable quantities.  
23 Study sites range from micro- to macro-tidal coastlines, spanning moderate  
24 to high energy beaches. The equilibrium model adopted here includes time  
25 varying terms describing both the magnitude and direction of shoreline re-  
26 sponse as a result of onshore/offshore sediment transport between the surf  
27 zone and the beach face. The model contains two coefficients linked to wave-  
28 driven processes: (1) the response factor ( $\phi$ ) that describes the ‘memory’ of  
29 a beach to antecedent conditions; and (2) the rate parameter ( $c$ ) that describes  
30 the efficiency with which sand is transported between the beach face and surf  
31 zone. Across all study sites these coefficients are shown to depend in a pre-  
32 dictable manner on the dimensionless fall velocity ( $\Omega$ ), that in turn is a sim-

---

K. D. Splinter, Water Research Laboratory, School of Civil and Environmental Engineering,  
UNSW Australia, Sydney, NSW, 2052, Australia (k.splinter@unsw.edu.au)

33 ple function of local wave conditions and sediment grain size. When tested  
34 on an unseen data set, the new equilibrium model with generalized forms of  
35  $\phi$  and  $c$  exhibited high skill (Brier Skills Score, BSS = 0.85).

## 1. Introduction

36 The world's coastlines mark the interface between the oceans and the continents. Along  
37 sandy, wave-dominated stretches of coast, this interface, denoted here as the shoreline, can  
38 be quite dynamic; moving landward (eroding) during periods of higher wave energy and  
39 moving seaward (accreting) during periods of lower wave energy. The ability to predict  
40 both the direction and magnitude of shoreline response to changing wave conditions, and  
41 therefore the temporal variability in shoreline position is of primary interest to coastal  
42 scientists and managers. In particular, predictive models are sought that can provide  
43 reliable estimates of the cumulative shoreline response to both short-term storms and  
44 longer-term changes in local wave climate.

45 One of the biggest challenges to achieving this is that the suite of predictive models  
46 presently available typically require site-specific calibration. In an effort to expand the  
47 general applicability of shoreline models at a wide range of sites where historical data is  
48 presently limited, we utilize 12 existing shoreline data sets (herein referred to as 'study  
49 sites') along six different stretches of coastline to examine the dependence of model coeffi-  
50 cients on environmental variables, such as local wave conditions and sediment grain size.  
51 This more generalized approach allows for new physical relationships to be derived from  
52 more readily available environmental parameters. The broad range of study sites, which  
53 include medium to high energy, micro- to meso-tidal environments encompass the major-  
54 ity of commonly observed wave-dominated sandy coastlines where shoreline modeling is  
55 most commonly applied.

56 The choice of model used to predict shoreline change will depend on the governing  
57 processes at the site and the timescales over which predictions are required. Both cross-  
58 shore and longshore sediment transport determine shoreline response to changing wave  
59 conditions. On open coastlines, longshore processes are commonly observed to act over  
60 much longer timescales (decades) and most often do not dominate the seasonal to annual  
61 shoreline variability [e.g. *Aubrey, 1979; Clarke and Eliot, 1988; Hansen and Barnard,*  
62 *2010; Ruggiero et al., 2010*]. Estimating decadal-scale (and beyond) shoreline change  
63 due to gradients in longshore transport is most commonly achieved using 1- (or n-) line  
64 models [e.g. *Pelnard-Considere, 1956; Hanson and Kraus, 1989; Ruggiero et al., 2010*]. In  
65 these n-line models, the cross-shore profile is assumed to maintain a constant shape and  
66 the alongshore gradients in longshore transport result in a cross-shore translation of the  
67 profile. *Ruggiero et al. [2010]* found their 1-line shoreline model was skillful at decadal-  
68 scale timescales, but had poor skill at the annual scale, which they hypothesized to be  
69 dominated by cross-shore processes.

70 At the other end of the temporal spectrum (i.e. individual storms), cross-shore processes  
71 tend to dominate the erosion response and several process-based models such as SBeach  
72 [*Larson and Kraus, 1989*] and XBeach [*Roelvink et al., 2009*] have been used to estimate  
73 storm response with an emphasis on quantifying erosion of the upper beach and dune [e.g.  
74 *Carley et al., 1999; McCall et al., 2010; Splinter and Palmsten, 2012; Splinter et al., 2014*].  
75 However, bathymetry (or profile) data is rarely available, and if it is, it is typical that it  
76 pre-dates the onset of a specific storm by several weeks to months (or even years), which  
77 can lead to large uncertainty in the modeled shoreline response [*Splinter and Palmsten,*

2012] and often necessitates ‘best guess’ tuning of model coefficients and limited capacity  
to apply at other coastal sites.

Encompassing the time frame between individual storms and decadal-scale trends (i.e. seasonal to multi-year) a number of data-driven [e.g. *Frazer et al.*, 2009; *Anderson et al.*, 2010; *Karunaratna and Reeve*, 2013], as well as equilibrium-based semi-empirical shoreline models [e.g. *Miller and Dean*, 2004a; *Davidson and Turner*, 2009; *Yates et al.*, 2009, 2011; *Davidson et al.*, 2010, 2013] have been used to model shoreline variability over timescales between individual storms and decadal-scale trends (i.e. seasonal to multi-year). These models require information on shoreline position sampled on the order of monthly and spanning at least two years to provide robust calibration of model coefficients [*Splinter et al.*, 2013b]. Most recently, *Pender and Karunaratna* [2013] proposed a method to extend the application of storm scale process models to longer (inter-annual) timescales. They employed a statistical process-based approach where they utilized a statistical framework [[Callaghan et al., 2008](#)] to model waves and were required to separately calibrate XBeach [*Roelvink et al.*, 2009] for the erosion and accretion phases in order to reproduce both phases of the shoreline response signal on inter-annual timescales.

The focus of this contribution is the application of equilibrium shoreline models to shoreline change driven by cross-shore processes over weekly to seasonal and multi-year timescales. A particular attraction of equilibrium models in this context is the relative transparency in the governing processes compared to data-driven models, and that they are also less sensitive than process-based models to uncertainty and/or errors in boundary conditions. Importantly, a growing number of authors [*Miller and Dean*, 2004a; *Davidson and Turner*, 2009; *Yates et al.*, 2009, 2011; *Davidson et al.*, 2010, 2013] have shown

101 that equilibrium-based shoreline models perform well at exposed, open coastlines where  
102 significant seasonal (i.e. summer - winter cycle) shoreline variability occurs.

103 However, not all models of this type have shown a similar degree of skill across a broad  
104 range of sites. Both *Miller and Dean* [2004a] and *Yates et al.* [2009] reported on some  
105 sites where their equilibrium-based models performed quite poorly. For example, the  
106 coarse sand beach at San Onofre, California showed minimal seasonal shoreline change  
107 despite the prevailing wave climate being similar to other beaches examined. This differ-  
108 ence was hypothesized by *Yates et al.* [2009] to be due to the coarser sediment on San  
109 Onofre having the effect of stabilizing the shoreline variability relative to other finer sand  
110 sites. While the model of *Yates et al.* [2009] does not explicitly include sediment grain  
111 size in its formulation, when the authors applied model coefficients derived from a signif-  
112 icantly higher energy beach but with similar coarse grain size (Ocean Beach, California),  
113 the model qualitatively reproduced the subdued seasonal fluctuations observed at San  
114 Onofre. It was concluded by *Yates et al.* [2011] that their model coefficients appeared  
115 to (implicitly) depend in part on sediment grain size, and this insight now informs the  
116 present contribution.

117 The equilibrium shoreline model proposed by *Davidson et al.* [2013] differentiates equi-  
118 librium response of varying beach types through the dimensionless fall velocity ( $\Omega$ ):

$$\Omega = \frac{H_{s,b}}{wT_p}, \quad (1)$$

119 where  $H_{s,b}$  is the significant breaking wave height,  $w$  is the settling velocity and is a  
120 function of the site-specific median grain size ( $d_{50}$ ), and  $T_p$  is the spectral peak wave period.

121 They applied the new model to two contrasting beaches on the east coast of Australia: a



122 20 km-long, exposed open beach with a dominant annual shoreline variability (Gold Coast,  
123 Queensland) and a 3.5 km-long, semi-embayed beach where the shoreline is observed to  
124 rapidly respond to individual storms throughout the year (Narrabeen-Collaroy, New South  
125 Wales). While the model was able to successfully reproduce the contrasting shoreline  
126 responses at both these sites, site-specific calibration was still required.

127 The reality is that the necessary data needed for robust model calibration of any sedi-  
128 ment transport model aimed at predicting seasonal to multi-year shoreline change is rarely  
129 available. *Long and Plant* [2012] recently proposed a new method for determining site-  
130 specific model coefficients. Utilizing an Extended Kalman Filter approach and a sensible  
131 starting estimate of model coefficient values, they were able to achieve model coefficient  
132 convergence on their synthetic test case using two years of monthly sampled data. How-  
133 ever, this method has yet to be successfully applied to field data, with one major limitation  
134 potentially being *a priori* knowledge of a reasonable first estimate of each model coeffi-  
135 cient. This contribution develops and presents a potential alternative solution. Starting  
136 from an existing equilibrium-based model for shoreline change described in further de-  
137 tail in Section 3, the calibration process is recast and model coefficients parameterized in  
138 terms of commonly available wave and sediment characteristics.

139 First we describe the study sites and compare the differing observations of inter-annual  
140 shoreline behavior (Section 2). This is followed by a brief description of the existing  
141 equilibrium shoreline model that provides the starting point for the analyses that follow  
142 (Section 3). Shoreline predictions based on site-specific calibration using available histor-  
143 ical shoreline data sets for each site are presented and compared in Section 4. Inter-site  
144 variability among model coefficients is then investigated leading to the derivation of gen-

145 eralized forms of model coefficients. Equilibrium shoreline response and the application  
146 of the new generalized model at an additional thirteenth site where minimal calibration  
147 data was available (i.e. a blind test ) is presented in Section 5. Finally, a summary of key  
148 study findings is provided in Section 6, along with encouragement for other researchers  
149 to now test the broader application of the generalized model at their specific beaches of  
150 interest (Matlab GUI provided on request).

## 2. Multi-site Observations

151 The 12 study sites used here to explore equilibrium beach response and inter-site pa-  
152 rameter variability were divided into two distinct categories: (1) exposed open coastlines;  
153 and (2) semi-embayed coastlines (Table 1). Sites were mainly limited to micro- and meso-  
154 tidal locations. Fundamentally, the selection and limitation to the use of these specific  
155 sites was based on the practical availability to the Authors of shoreline time series of a  
156 minimum of five years duration, sampled at a minimum monthly interval and co-located  
157 to suitable wave data. Three sites utilized video-derived [e.g. Argus: *Holman et al.*, 2003]  
158 shorelines, while the remaining nine were collected using standard survey techniques, such  
159 as RTK-GPS. Where possible, shoreline data was alongshore averaged (Table 2) to limit  
160 the influence of local short-scale alongshore variability (e.g. beach and/or mega cusps).  
161 The study site locations are shown in Figure 2 and comprise of two stretches of coastline  
162 in Australia, three in the United States, and one in France. Characteristics of each site  
163 are summarized in Tables 1 and 2 and discussed in more detail below.

164 Three summary environmental statistics for each site are reported in Table 1. The  
165 first is the temporal mean (over the record of available data) of the dimensionless fall  
166 velocity ( $\Omega$ , eq. 1). The temporal mean ( $\overline{\Omega}$ ) can be used to infer the dominant (modal)

167 beach state after *Wright and Short* [1984]. The remaining two are based on the standard  
 168 deviation of  $\Omega$  at yearly (defined by a calendar year and denoted as  $\sigma_{\Omega_{360}}$ ) and monthly  
 169 (defined by a calendar month and denoted as  $\sigma_{\Omega_{30}}$ ) intervals. The temporal mean of these  
 170 statistics over the entire record length ( $\bar{\sigma}_{\Omega_{360}}, \bar{\sigma}_{\Omega_{30}}$ ) is then determined for each site. The  
 171 mean yearly standard deviation ( $\bar{\sigma}_{\Omega_{360}}$ ) characterizes the variability in the forcing wave  
 172 climate over a year, while the mean monthly standard deviation ( $\bar{\sigma}_{\Omega_{30}}$ ) characterizes the  
 173 variability at the timescales of individual storms. It is expected that  $\bar{\sigma}_{\Omega_{360}}/\bar{\sigma}_{\Omega_{30}} \geq 1$ . A  
 174 large ratio of  $\bar{\sigma}_{\Omega_{360}}/\bar{\sigma}_{\Omega_{30}}$  indicates a site that is dominated by seasonal fluctuations in wave  
 175 steepness. As the ratio of  $\bar{\sigma}_{\Omega_{360}}/\bar{\sigma}_{\Omega_{30}}$  approaches unity, we expect a site that experiences  
 176 both high and low steepness waves throughout the year (i.e., a storm-dominated site) and  
 177 a shoreline time series that mirrors this. The ratio can be used to characterize site-specific  
 178 beach state. Higher-energy beaches with a dominant seasonal cycle ( $\bar{\sigma}_{\Omega_{360}}/\bar{\sigma}_{\Omega_{30}} > 1$ ) are  
 179 anticipated to remain more stable and in a higher energy state, while more intermediate  
 180 and low energy sites with a large variability in wave conditions at shorter timescales  
 181 ( $\bar{\sigma}_{\Omega_{360}}/\bar{\sigma}_{\Omega_{30}} \sim 1$ ) will likely respond quickly to storms and more rapidly return to these  
 182 lower energy states. To encapsulate these differing physical behaviors, a weighted mean  
 183 dimensionless fall velocity ( $\bar{\Omega}_r$ ) is derived:

$$\bar{\Omega}_r = \bar{\Omega} \frac{\bar{\sigma}_{\Omega_{360}}}{\bar{\sigma}_{\Omega_{30}}}. \quad (2)$$

## 2.1. Exposed Open Coastlines

### 2.1.1. Benson Beach (North Head), Washington, USA

184 Benson Beach is a 3 km long, fine sand ( $d_{50} \sim 0.2$  mm) exposed beach (Tables 1 and  
 185 2), located between the North Head headland and the north jetty of the Columbia River.  
 186

187 The site is meso-tidal with a mean spring tide range ( $\Delta\text{Tide}$ ) of 2.3 m (Table 2). The  
188 nearshore is characterized by a multi-bar system (typically between 2 and 4 sandbars) and  
189 is the most dissipative site available to this study (Figure 1), with  $\bar{\Omega} = 12.38$  (Table 1).  
190 During the summer, the inner sandbar moves onshore and attaches to the shoreline, while  
191 in the winter, the beach face is cut and sand is transported offshore to the sandbars. Both  
192 the shoreline and the wave climate exhibit a highly seasonal and well-correlated signal  
193 [*Ruggiero et al.*, 2009]. Longshore transport is estimated at 0.4M m<sup>3</sup>/yr to the north.  
194 Winter waves (and storms) are typically from the NW, while the smaller summer waves  
195 generally arrive from the SW. The mean yearly standard deviation in dimensionless fall  
196 velocity ( $\bar{\sigma}_{\Omega_{360}}$ ) is 4.48 and the mean monthly standard deviation in dimensionless fall  
197 velocity ( $\bar{\sigma}_{\Omega_{30}}$ ) is 3.69. This highly seasonal site has a ratio of  $\bar{\sigma}_{\Omega_{360}}/\bar{\sigma}_{\Omega_{30}} = 1.21$ , which is  
198 the second highest of all sites examined, resulting in a weighted mean dimensionless fall  
199 velocity ( $\bar{\Omega}_r$ ) = 15.04.

200 Dredge material was placed within the inter-tidal system near the jetty in the summers  
201 of 2008 ( $\sim 96,000$  m<sup>3</sup>) and 2010 ( $\sim 281,000$  m<sup>3</sup>). Analysis of the dredge material indi-  
202 cates the sand was moved offshore forming a new sandbar shortly after placement during  
203 the first storm and that the MHW shorelines during and post placement lie within the  
204 natural envelope of shoreline variability at this site. To limit the impact on the analysis  
205 presented below of these localized nourishments, as well as the presence of the jetty, this  
206 study utilized the 1 km alongshore averaged mean high water (MHW) shoreline centered  
207 approximately 2 km north of the jetty (Table 2). Wave data (86%) was obtained from  
208 wave buoy NDBC 46029 (Columbia River Bar) located in 145 m of water and gap-filled  
209 with NDBC 46041 (Cape Elizabeth) located in 114 m of water. These buoys were chosen

210 as they are considered deep water for periods ( $T_p$ ) less than 12 seconds (65% of the data)  
211 and they cover the entire monitoring period of the North Head site. The correlation be-  
212 tween the two buoys for wave height was  $R = 0.95$ . Further information about this site  
213 can be obtained at [www.planetargus.com/north\\_head](http://www.planetargus.com/north_head).

### 214 **2.1.2. Truc Vert, France**

215 Truc Vert is a medium-grained ( $d_{50} \sim 0.3$  mm [*van Rooijen et al.*, 2012]), sandy beach  
216 located in the southwest of France. The site is meso- to macro-tidal, with a mean spring  
217 tide range ( $\Delta\text{Tide}$ ) of 3.7 m and a moderate wave climate ( $\bar{\Omega} = 6.19$ , Tables 1 and  
218 2). There exists a strong seasonal dependence in waves ( $\bar{\sigma}_{\Omega_{360}} = 2.70$ ) and the resulting  
219 position of the MHW shoreline. The ratio of  $\bar{\sigma}_{\Omega_{360}}/\bar{\sigma}_{\Omega_{30}}$  is 1.22, and is the highest for all  
220 sites included in this study. The weighted  $\bar{\Omega}_r$  is 7.55. The beach morphology (Figure 1) is  
221 typically double-barred, with the inner, intertidal sandbar classified as transverse bar and  
222 rip [*Senechal et al.*, 2009] and the outer bar as crescentic [*Castelle et al.*, 2007a]. Around  
223 Truc Vert Beach, the longshore drift is about  $0.3 \text{ M m}^3/\text{yr}$  with a negligible alongshore  
224 variability along this stretch of coastline suggesting a limited influence of the longshore  
225 transport on the overall shoreline evolution [*Idier et al.*, 2013].

226 MHW shorelines were derived from topographic survey data, which were sampled every  
227 2-4 weeks (Table 2), with a 1-year gap in 2008 [*Castelle et al.*, 2014]. The MHW contour  
228 was alongshore averaged over the extent of the available survey data to minimize the local  
229 influence of mega cusps. Between 2003 and 2008, the alongshore extent of the surveys was  
230 350 m, and was extended to 750 m in 2008 and then again to 1200 m in 2012 [*Castelle*  
231 *et al.*, 2014]. Wave data at this site was based on modeled WaveWatchIII output every 3  
232 hours from grid point  $1^\circ 30' \text{ W}$ ,  $44^\circ 30' \text{ N}$ , which is located 34 km SW of the study site in

233 70 m water depth. *Davidson et al.* [2011] tested a similar form of the shoreline model used  
234 here and found that temporally degrading the wave data (i.e. increasing the time step) by  
235 up to 2 days did not cause a significant decrease in model skill at the sites tested. As such,  
236 using the 3-hourly WaveWatchIII output in the absence of hourly measured buoy data at  
237 this site is acceptable. The 11.5 years of WWIII data is corrected via linear regression fit  
238 with approximately 5 years of interspersed buoy data located in 54 m of water as detailed  
239 in *Castelle et al.* [2014].

### 240 **2.1.3. Narrowneck (Gold Coast), Queensland, Australia**

241 The Gold Coast is located along the east coast of Australia near the Queensland - New  
242 South Wales state border. The Gold Coast site is a micro-tidal ( $\Delta\text{Tide} = 1.5$  m), medium  
243 sand size ( $d_{50} \sim 0.25$  mm), 20 km long, straight beach, exposed to waves from a range of  
244 directions (Tables 1 and 2). The site is located approximately 2 km up-drift (south) of an  
245 artificial surfing reef and outside the influence of this nearshore structure. Predominant  
246 wave direction is from the south-east and results in an estimated average net northerly  
247 longshore transport at Narrowneck of  $0.5\text{M m}^3/\text{yr}$  [*Delft*, 1970; *Patterson*, 2007], however,  
248 this can vary significantly from year to year [*Patterson*, 2007; *Splinter et al.*, 2012]. On  
249 average, summer waves are smaller and more easterly, while winter waves are larger and  
250 have a larger southerly component. The wave climate of the SE coast of Australia is  
251 influenced by ENSO time scale phenomena, as well as extreme storms, such as East Coast  
252 Lows and tropical cyclones [*Allen and Callaghan*, 1999].

253 The nearshore morphology at this site is typically a double-barred system [*van Enckevort*  
254 *et al.*, 2004] and ranges from alongshore-uniform sandbars during high wave events to  
255 crescentic bars and rip dominated low tide terraces under prolonged mild wave conditions

(Figure 1). Shoreline variability along the Gold Coast displays an annual cyclic pattern related to changes in seasonal mean wave height ( $\bar{\sigma}_{\Omega_{360}} = 2.08$ ) [Davidson and Turner, 2009; Splinter et al., 2011b]; however, since 2005 there has been an observed shift in shoreline variability from a predominant seasonal pattern to more storm driven with episodic erosion (Figure 4). While  $\bar{\Omega} = 6.17$  at the Gold Coast is comparable to that at Truc Vert, this site has a larger storm-dominated standard deviation, and the second lowest ratio of  $\bar{\sigma}_{\Omega_{360}}/\bar{\sigma}_{\Omega_{30}} = 1.13$  among the exposed sites examined, resulting in  $\bar{\Omega}_r = 6.95$ . Weekly mean sea level (MSL) shorelines (Table 2) were derived from video images and averaged over a 1 km length of coastline to limit the influence of local rip-horn variability. Wave data for this study was obtained from the Gold Coast buoy located in 18 m of water directly offshore from this study site.

#### 2.1.4. Ocean Beach, California, USA

Ocean Beach is a 7 km, west facing, medium-grained ( $d_{50} \sim 0.3$  mm), micro-tidal ( $\Delta\text{Tide} = 1.83$  m), sandy beach located directly south of the entrance to San Francisco Bay (Tables 1 and 2). The site is swell dominated and exposed to strong alongshore tidal currents due to tidal movement in and out of the Bay [Barnard et al., 2012]. Tidal currents are generally larger at the north end of Ocean Beach (transects north of OB10), while waves generally have a larger impact on the southern section of the beach [Barnard et al., 2012], which contains an erosion hotspot (i.e. an area of increased erosion compared to the surrounding beach) between transects OB3 and OB4 [Barnard et al., 2012]. The majority ( $\sim 45\%$ ) of the waves are from the northwest ( $300^\circ - 330^\circ\text{N}$ ), however 50% of winter waves (Nov-March) are from the west ( $270^\circ - 300^\circ\text{N}$ ) and in the summer, long period swell can occasionally also come from the S-SW ( $180^\circ - 210^\circ\text{N}$ ) [Eshleman et al.,

279 2007] with an  $\bar{\Omega} \sim 5.25$ . Ocean Beach is strongly controlled by gradients in longshore  
280 transport [*Hansen et al.*, 2013b], however, those gradient patterns only seem to change on  
281 multi-decadal timescales, primarily as a result of the large scale changes of the ebb-tidal  
282 delta morphology [*Hansen et al.*, 2013a]. Longshore transport has been roughly estimated  
283 in the area to be between 0.1 and 0.3 M m<sup>3</sup>/yr, however, over the timescale considered  
284 here, cross-shore processes dominate the seasonal to sub-decadal shoreline response.

285 To minimize the potential influence of a known erosion hotspot [*Hansen and Barnard*,  
286 2010] at the southern end of Ocean Beach and the strong tidal currents at the north  
287 end of this site, the analysis presented here focuses on the central 2 km of the beach  
288 around transects OB5 and OB8 as presented in *Yates et al.* [2011]. The MHW contour  
289 was extracted from available survey data and alongshore averaged over a 500 m section  
290 for each of the transects to remove the influence of localized alongshore variability and to  
291 conform with similar work at this site by *Yates et al.* [2011](Table 2). Available wave data  
292 is sourced from the deep water CDIP 029 buoy located approximately 80 km west of Ocean  
293 Beach. Local waves are influenced by the Fallon Islands (40 km west) and a substantial  
294 ebb tidal delta ( $\sim 150$  km<sup>2</sup>) at the mouth of the Bay, which have been observed to cause  
295 substantial alongshore gradients in wave energy [*Eshleman et al.*, 2007; *Hansen et al.*,  
296 2013b]. To account for these features, an existing look-up table derived from a calibrated  
297 SWAN output presented in *Eshleman et al.* [2007] and *Hansen et al.* [2013b] and verified  
298 in *Eshleman et al.* [2007] against inshore observations was used here to transform the  
299 deepwater waves into the -10 m contour directly offshore of OB5 and OB8. The shoreline  
300 and inshore wave data vary on a seasonal time scale ( $\bar{\sigma}_{\Omega_{360}} \sim 1.75$ ). Ocean Beach has a



301 larger ratio of  $\bar{\sigma}_{\Omega_{360}}/\bar{\sigma}_{\Omega_{30}} \sim 1.18$  and is mid-range among all the exposed sites examined,  
302 resulting in a weighted mean dimensionless fall velocity of  $\bar{\Omega}_r \sim 6.2$ .

### 303 **2.1.5. USACE Field Research Facility, Duck, NC, USA**

304 The beach at Duck is an east facing, intermediate ( $\bar{\Omega} = 5.06$ ), micro-tidal ( $\Delta\text{Tide} =$   
305 1.2m), medium-grained ( $d_{50} \sim 0.2\text{-}0.3$  mm) open exposed coastline located on the Outer  
306 Banks of North Carolina. The area experiences a net southerly littoral drift; however, the  
307 wave climate typically has a seasonal signal, with smaller waves during the summer months  
308 typically arriving from the southeast and larger, winter waves arriving from the northeast.  
309 The area can be impacted by hurricanes in late summer - early fall and large winter storms  
310 (Nor'easters) that can cause significant storm surge and erosion. The annual standard  
311 deviation in the dimensionless fall velocity ( $\bar{\sigma}_{\Omega_{360}} = 2.61$ ) is similar to that observed at the  
312 Truc Vert site, but also has one of the largest storm-scale variability standard deviations  
313 ( $\bar{\sigma}_{\Omega_{30}} = 2.35$ ). As a result, the ratio of  $\bar{\sigma}_{\Omega_{360}}/\bar{\sigma}_{\Omega_{30}} = 1.11$  at the Duck site is the lowest of  
314 all exposed open coastlines available to this study, resulting in  $\bar{\Omega}_r = 5.61$  (Table 1). The  
315 nearshore morphology (Figure 1) is typically double-barred, dynamic, and ranges from  
316 low tide terraces to alongshore uniform sandbars [*Lippmann and Holman, 1990*].

317 The beach at Duck is the most complex site utilized in this study due to both natural and  
318 anthropogenic influences on the shoreline. In addition to the influence of hurricanes and  
319 large Nor'easter storms, located at this site is a 560 m-long research pier that significantly  
320 influences the nearshore morphology and sediment transport immediately adjacent [e.g.  
321 *Miller and Dean, 2004a*]. Both longshore and cross-shore processes influence the shoreline.  
322 *Plant et al. [1999]* and *Miller and Dean [2003]* observed an increasing alongshore uniform  
323 component of variability with distance offshore, and that the shoreline was dominated by

324 variability at timescales greater than one year. The shoreline is considered to be stable  
325 over the long-term [*Birkemeier et al.*, 1985] with a mean annual range in cross-shore  
326 shoreline position less than 3 m [*Alexander and Holman*, 2004].

327 The profile data used in this study was collected at the US Army Corps of Engineers  
328 Field Research Facility (USACE FRF). The survey area extends approximately 600 m on  
329 either side of the FRF pier, however, to minimize the more localized influences of the pier  
330 on shoreline data, only the MHW shorelines that were at least 350 m south of the pier  
331 were used and alongshore averaged over 250 m (Table 2). Previous analysis by *Miller and*  
332 *Dean* [2004a] of the Duck profile data from 1981 - 2002 indicated that roughly 70% of the  
333 observed shoreline variability over this 250 m section was alongshore uniform. Wave data  
334 was obtained from the FRF 17 m buoy (55%) and gap-filled with NDBC 44014 (Virginia  
335 Beach) located in 95 m of water. Waves from the FRF 17m buoy were reverse shoaled  
336 to deep water prior to gap filling for consistency. The correlation of wave height between  
337 the two data sets was  $R = 0.59$ .

## 2.2. Semi-Embayed Coastlines

### 338 2.2.1. Narrabeen and Collaroy, NSW, Australia

339 Narrabeen and Collaroy beaches are located on the Northern Beaches region of Sydney.  
340 The beaches are micro-tidal ( $\Delta\text{Tide} = 2$  m), coarse sand ( $d_{50} \sim 0.4$  mm), east facing,  
341 swash-aligned and occur within a single 3.5 km embayment (Tables 1 and 2). The two  
342 adjacent beaches are bounded by prominent rocky headlands: Warriewood Headland to  
343 the north and Long Reef Headland to the south. The beaches are storm-dominated, with  
344 the northern (Narrabeen) end exposed to, and the southern (Collaroy) end sheltered from,  
345 the predominant south to south-easterly wave climate. An alongshore gradient in wave

energy within the embayment exists resulting in  $\bar{\Omega}$  ranging from 3.08 at the southern end  
of Collaroy beach to 4.08 at the northern end of Narrabeen beach. Typically, the smaller,  
summer waves have a more easterly component than the larger, more southerly winter  
waves, similar in this respect to Narrowneck (Section 2.1.3). The ratio of  $\bar{\sigma}_{\Omega_{360}}/\bar{\sigma}_{\Omega_{30}}$   
 $= 1.07$  is the lowest among all the study sites included here and highlights the larger  
storm (short-term) contribution of wave variability along Narrabeen-Collaroy (Table 1).  
The weighted mean dimensionless fall velocity around the embayment is within the most  
dynamic intermediate range ( $3.28 \leq \bar{\Omega}_r \leq 4.37$ ). Hourly wave data was obtained from  
the Sydney buoy located in 74 m water depth, 11 km SE of the site. To account for wave  
refraction into the embayment and the resulting alongshore gradient in wave height, these  
offshore observations were then used as input into a look-up table of calibrated SWAN  
modeled output at the -15 m contour around the embayment.

The beach morphology within the Narrabeen-Collaroy embayment is dynamic, ranging  
from dissipative, with a longshore uniform sandbar during major storms, through all four  
intermediate beach states (Figure 1) during milder wave conditions. Five profile locations  
along the embayment have been consistently surveyed on a monthly basis using standard  
survey techniques since 1974 at historical profiles PF1, PF2, PF4, PF6 and PF8; however,  
the necessary directional wave data is only available since 1992. To be consistent with the  
timespan of all data sets available to this study (2000s), profile data over a 7-year period  
coinciding with the availability of Argus camera-derived shorelines (NB2600) was used  
here (Table 2). The profile data utilizes the MHW contour, is not alongshore averaged  
and sampled monthly. In contrast, the Argus MHW shoreline is sampled weekly and  
alongshore averaged over 400 m to limit the influence of small scale alongshore variability.

369 Comparing sites PF6 and NB2600 (Figure 5), which overlap the same alongshore location,  
370 the reader can see short-lived accretionary events (e.g. mid-2010) that are present in the  
371 profile data (PF6) but have been averaged out by the alongshore smoothing in NB2600.  
372 As a benchmark, the average alongshore standard deviation of the shoreline at NB2600  
373 was 1.5 m, which if applied at each profile within the embayment, would add an additional  
374 3 m of uncertainty onto the shoreline position.

375 It has been previously observed that both cross-shore and alongshore transport pro-  
376 cesses influence shoreline position within the Narrabeen-Collaroy embayment at annual  
377 and longer (i.e. ENSO) timescales [*Short and Trembanis, 2004; Ranasinghe et al., 2004*].  
378 *Harley et al. [2011]* has shown that at Narrabeen-Collaroy, 60% of the observed shoreline  
379 variance is due to cross-shore processes (the first EOF) linked to the temporal variation  
380 of wave height and 26% of the shoreline variance is linked to longshore processes (beach  
381 rotation in the second EOF). PF1 is the most exposed site and is located at the north end  
382 of Narrabeen. PF4 is located near the centre of the embayment and the pivot point of  
383 observed embayment rotation [*Harley et al., 2011*] and as such, cross-shore process have  
384 been previously assumed to be the driving factor in shoreline change. PF8 is the most  
385 sheltered and southern location at Collaroy considered.

### 3. An Equilibrium-based Shoreline Model: *ShoreFor*

#### 3.1. Formulation

386 The *ShoreFor* model was first presented in *Davidson et al. [2013]* and is used here  
387 as the basis to explore the more general applicability of equilibrium shoreline modeling  
388 and inter site comparison of model coefficients. *ShoreFor* is based upon the principal that  
389 cross-shore dominated shorelines migrate towards a time varying equilibrium position [e.g.

390 *Miller and Dean, 2004a; Davidson and Turner, 2009; Yates et al., 2009; Davidson et al.,*  
 391 *2010*]. By this approach, the rate of shoreline change ( $dx/dt$ , m/s) is simply defined as:

$$\frac{dx}{dt} = c(F^+ + rF^-) + b. \quad (3)$$

392 The rate of shoreline change model (eq. 3) includes two wave-driven coefficients ( $c$ ,  $\phi$ )  
 393 and a linear trend term ( $b$ ). The first wave-driven parameter is the rate parameter ( $c$ ;  
 394  $\text{m}^{1.5}\text{s}^{-1}\text{W}^{-0.5}$ ). The second wave-driven parameter is the response factor ( $\phi$ ; days) that  
 395 is optimized during the calculation of the equilibrium dimensionless fall velocity ( $\Omega_{eq}$ , eq.  
 396 8) described below. The linear term ( $b$ ; m/s) is included here to acknowledge longer-  
 397 term processes not explicitly included in the present form of the model (e.g. gradients in  
 398 longshore transport, cross-shelf sand supply, etc), which may be captured by a constant  
 399 rate over long time frames. Where these processes cannot be captured by the linear term  
 400 (or the wave driven component), the model does not resolve the shoreline response.

401 The key forcing term in (3) is subdivided into accretionary ( $F^+$ ) and erosional ( $F^-$ )  
 402 components multiplied by a ratio ( $r$ , no units) to encapsulate that accretionary and erosion  
 403 responses are governed by different processes [*Miller and Dean, 2004a; Yates et al., 2009;*  
 404 *Splinter et al., 2011a*]. For clarity,  $r$  will be referred to as the erosion ratio as it is attached  
 405 to the erosion forcing term ( $F^-$ ). The erosion ratio is not a free model coefficient, but  
 406 determined within the model based on the balance between accretion and erosion forcing  
 407 ( $F$ ,  $(\text{W}/\text{m})^{0.5}$ ) such that no trend in the integrated forcing results in no trend in the  
 408 shoreline evolution due to cross-shore transport processes. The erosion ratio in (3) is  
 409 numerically evaluated in the model as:

$$r = \left| \frac{\sum_{i=0}^N \langle F_i^+ \rangle}{\sum_{i=0}^N \langle F_i^- \rangle} \right|, \quad (4)$$

410 where  $||$  indicates the absolute value,  $\langle \rangle$  indicates a numerical operation that removes the  
 411 linear trend but preserves the record mean and  $N$  is the total record length.

412 The rate of shoreline response ( $dx/dt$ ) is dependent on the magnitude of forcing (i.e.  
 413 wave energy flux,  $P$ ) available to move sediment and the direction of shoreline response is  
 414 based on the disequilibrium (the deviation between the present and equilibrium position).  
 415 The forcing term ( $F$ ) is defined as:

$$F = P^{0.5} \frac{\Delta\Omega}{\sigma_{\Delta\Omega}}, \quad (5)$$

416 where  $P$  (Watts) is the breaking wave energy flux:

$$P = EC_g. \quad (6)$$

417  $E = 1/16\rho g H_{s,b}^2$  (Newton/m) is the significant wave energy at breaking (assuming a  
 418 breaking parameter,  $\gamma = 0.78$ ) and  $C_g = \sqrt{gh_b}$  is the shallow water group velocity (m/s),  
 419 where  $h_b$  (m) is the depth at breaking defined as  $h_b = H_{s,b}/\gamma$ . As described in *Davidson*  
 420 *et al.* [2013], *Davidson et al.* [2010] showed that results were not sensitive to the exponent  
 421 on  $P$  (i.e. 0.5) in equation 5, therefore it was sensibly chosen to agree with previous work,  
 422 such as *Yates et al.* [2009] whereby the shoreline rate of change is linearly related to the  
 423 wave height ( $H$ ).

424 The dimensionless fall velocity disequilibrium term ( $\Delta\Omega$ ) in (5) is given by:

$$\Delta\Omega = \Omega_{eq} - \Omega, \quad (7)$$

425 and is a function of the time varying equilibrium condition ( $\Omega_{eq}$ , eq. 8) and the instan-  
 426 taneous dimensionless fall velocity ( $\Omega$ , eq. 1). Note that the standard deviation of  $\Delta\Omega$   
 427 (denoted  $\sigma_{\Delta\Omega}$ ) is used to normalize  $\Delta\Omega$  in (5), such that the rate parameter ( $c$ ) and wave  
 428 energy flux ( $P$ ) determine the magnitude of the shoreline response ( $dx/dt$ ), rather than  
 429  $\Delta\Omega$ . The sign of  $\Delta\Omega$  determines the direction of shoreline change (erosion or accretion)  
 430 and is used to partition  $F^+$  and  $F^-$  in (3) and (4).

431 While *ShoreFor* is an equilibrium shoreline model, the time varying equilibrium position  
 432 ( $\Omega_{eq}$ , eq. 8) is based on beach state (rather than a shoreline position). Therefore, changes  
 433 in  $\Omega_{eq}$  directly link surf zone onshore-offshore sediment transport to the resulting shoreline  
 434 response. Following the approach outlined in *Davidson et al.* [2013], the time varying  
 435 equilibrium beach state was based on the formulation proposed by *Wright et al.* [1985]:

$$\Omega_{eq} = \left[ \sum_{i=1}^{2\phi} 10^{-i/\phi} \right]^{-1} \sum_{i=1}^{2\phi} \Omega_i 10^{-i/\phi}, \quad (8)$$

436 where  $i$  is the number of days prior to the present time and the response factor ( $\phi$ ) is a  
 437 model coefficient. The response factor represents the number of days in the past when the  
 438 weighting factor decreases to 10%, 1%, and 0.1% at  $\phi$ ,  $2\phi$ , and  $3\phi$  days prior to present  
 439 day. The present formulation incorporates all past beach state information for the past  $2\phi$   
 440 days (i.e. with a minimum weighting factor of 1%). Therefore, the equilibrium condition  
 441 ( $\Omega_{eq}$ ) is constantly evolving and maintains a weighted ‘memory’ of antecedent surf zone  
 442 and shoreline conditions.

443 Additionally, a representative response factor ( $\phi_r$ , days), is included here for compari-  
 444 son with other studies where a running mean is more commonly used. The representative

445 response factor is determined by transforming the weighted filter used in (8) to the equiv-  
 446 alent filter length if a running mean were used:

$$\phi_r = \left[ \sum_{i=1}^{2\phi} 10^{-i/\phi} \right]^{-1} \sum_{i=1}^{2\phi} [0 : dt : 2\phi] 10^{-i/\phi}. \quad (9)$$

447 For the purpose of inter-site comparison of model coefficients, wave energy flux ( $P$ ,  
 448 eq. 6) and dimensionless fall velocity ( $\Omega$ , eq. 1) were calculated using the depth-limited  
 449 significant breaking wave height ( $H_{s,b}$ ) since this is judged to best represent the local wave  
 450 forcing that is assumed to drive cross-shore shoreline change at each site. At the two sites  
 451 (Ocean Beach, CA, USA and Narrabeen, NSW, Australia) where significant refraction and  
 452 alongshore variation in wave height was expected, SWAN modeling was used to refract  
 453 waves inshore. To standardize the method used to determine wave-breaking statistics  
 454 at all sites, waves were first reverse-shoaled to deep-water from their respective depths  
 455 (Table 1) and then breaking wave height ( $H_{s,b}$ ; m), applying shoaling only, was calculated  
 456 following *Komar* [1974]:

$$H_{s,b} = 0.39g^{1/5}(T_p H_{o,s})^{2/5}, \quad (10)$$

457 where  $g$  ( $\text{m/s}^2$ ) is the acceleration due to gravity, and  $H_{o,s}$  (m) is the deep-water sig-  
 458 nificant wave height. On swell dominated coasts with large seasonal variations in  $T_p$  as  
 459 is observed along the California coastline, utilizing the breakpoint, rather than the deep  
 460 water conditions, can shift the temporal variability of the magnitude in breaking wave  
 461 heights at a beach and must be considered.



### 3.2. Model Expectations and Limitations

462 The model formulation presented above describes the temporal variation in shoreline  
463 position due to changing wave conditions, and as such, is best suited for locations where  
464 waves are the primary driver of shoreline response. The model does not account for  
465 short-scale processes such as alongshore variable bar welding, beach cusp formation, or  
466 rip embayments/horns. As such, sites where shoreline data can be alongshore averaged to  
467 limit the impact of these short-scale processes are preferred. Sheltered coastlines, or those  
468 that experience large tidal variation are also influenced by the changes in mean water  
469 level not included in the present form of the model. The exclusion of water level also  
470 precludes the impacts of changes in mean water level due to climatological impacts, such  
471 as storm surge, El-Nino Southern Oscillation (ENSO), and sea level rise. Where these  
472 processes potentially have a constant linear impact on shoreline change (e.g. sea level rise),  
473 these can be modeled by the linear trend term ( $b$ ). Shoreline change due to gradients in  
474 longshore transport and/or onshore/offshore feeding/loss of sand may also be captured in  
475 the present formulation by the linear trend term, however, there is no discrimination of  
476 the impact of these processes on shoreline change from each other. When these processes  
477 are not constant in time (such as multi-decadal embayment rotation), this variability is  
478 not accurately modeled. As such, it is anticipated this modeling approach is best suited  
479 on open micro- to meso-tidal coastlines, exposed to waves over time frames of years to  
480 decades.

### 4. Model Results

481 In this section we present the site-specific calibration of model coefficients and the overall  
482 skill of the generic equilibrium shoreline model at each of the 12 study sites followed by

483 the derivation of model coefficients using easily obtainable site information such as waves  
 484 and sediment grain size. Figure 3 provides a summary of these results. As the focus  
 485 of this work is inter-site comparison of model coefficients, the full available data set at  
 486 each site was used for model calibration. For a more detailed discussion on model skill  
 487 in relation to calibration length and validation on unseen data, the reader is referred to  
 488 *Davidson et al.* [2013] and *Splinter et al.* [2013b].

489 Three summary statistics are presented in Table 4 and are all based on a nominal 30-day  
 490 sampling interval to facilitate unbiased inter-site comparison. The first parameter used  
 491 for inter-comparison is Correlation ( $R$ ) between observed shoreline time series and model  
 492 predictions. The second method uses the Brier Skills Score [*Sutherland and Soulsby*, 2003]  
 493 and takes into account measurement error in the data ( $\Delta x$ ):

$$\text{BSS} = 1 - \frac{\sum [|x - x_m| - \Delta x]^2}{\sum (x - x_b)^2}, \quad (11)$$

494 where  $x$  is the observed shoreline,  $x_m$  is the modeled shoreline, and  $x_b$  is the baseline  
 495 model. Here we use  $x_b$  equal to the linear trend of the data in order to determine when  
 496 model skill is truly due to the model capturing the shoreline response due to varying  
 497 cross-shore wave processes, rather than the simple linear trend (i.e. the time integration  
 498 of  $b$  in (3)). Positive BSS indicates the model is an improvement over the baseline linear  
 499 trend, and descriptive skill values exceeding 0 are summarized in Table 3.

500 The third metric reported in Table 4 is the normalized mean square error (NMSE) that  
 501 compares the error variance to the observed variance. NMSE is chosen over root mean  
 502 square error (RMSE) as the individual data-model results are normalized by the variance  
 503 of the observations ( $x$ ) at each site, thereby providing a superior method for inter-site

504 comparison. Here the formula utilized by *Miller and Dean* [2004b] and *Splinter et al.*  
 505 [2013b] is adopted:

$$\text{NMSE} = \frac{\sum (x - x_m)^2}{\sum x^2}. \quad (12)$$

506 A value of  $\text{NMSE} = 0$  indicates the model perfectly captures all data points, while a  
 507  $\text{NMSE} = 1$  indicates the error variance (numerator in eq. 12) is equal to the variance of  
 508 the observations (denominator in eq. 12) and therefore the model has no skill. Similar to  
 509 the BSS, a range of descriptive NMSE skill is summarized in Table 3.

#### 4.1. Exposed Open Coastlines

510 With the exception of the Duck data set, the observed shorelines from the remaining five  
 511 exposed sites exhibit a strong seasonal signal with larger waves driving shoreline erosion  
 512 and beach recovery (shoreline accretion) during prolonged periods of lower steepness waves  
 513 (Figure 4). The *ShoreFor* equilibrium model characteristically performed well at these  
 514 five exposed beach sites, with Correlation ( $R$ ) typically exceeding 0.8 (Figure 3), and skill  
 515 classified as ‘excellent’ (Table 3) based on BSS and ‘good’ based on NMSE (Table 4).  
 516 Encouragingly, the equilibrium shoreline model, *ShoreFor*, captured the strong seasonal  
 517 signal observed at five of the sites, as well as the contrasting anomalous years at North  
 518 Head (i.e. 2009, Figure 4). From 2005 until the end of the available monitoring in 2008,  
 519 the Gold Coast site appears to have transitioned from a seasonally-dominated shoreline  
 520 to one that experiences more episodic erosion (Figure 4). The large erosion event in 2006  
 521 is linked to a cluster of storms together with the onset of a new net offshore migration  
 522 event and outer bar decay [*Castelle et al.*, 2007b; *Ruessink et al.*, 2009]. Further analysis  
 523 is needed to confirm if a second erosional event combined with a net offshore migration

524 and bar decay occurred in 2008. The equilibrium-based model is still capable of capturing  
 525 this transition, however the magnitude of storm response is not always captured and the  
 526 model marginally lags response post 2005.

527 Three of the exposed beach sites: Gold Coast ( $\bar{\Omega} = 6.14$ ); Truc Vert ( $\bar{\Omega} = 6.02$ ); and  
 528 North Head ( $\bar{\Omega} = 12.56$ ) had optimized response factors ( $\phi$ ) close to 1000 days (Figure 3),  
 529 equating to representative response factors ( $\phi_r$ , eq. 9) around 400 days. Recalling that  $\phi_r$   
 530 represents the equivalent number of days in the past that is used in a running mean filter  
 531 of the wave data to determine the equilibrium condition. This indicates the equilibrium  
 532 condition (eq. 8) is roughly equal to the annual mean dimensionless fall velocity and that  
 533 the observed dominant signal of shoreline variability and the rate of cross-shore sediment  
 534 exchange at these locations is primarily driven by seasonal (or longer) variability in wave  
 535 steepness oscillating about this mean (Figure 4). The two California sites at Ocean Beach  
 536 ( $\bar{\Omega} = 5.18 - 5.26$ ), along with the Duck site ( $\bar{\Omega} = 5.06$ ) had optimized  $\phi$  values between  
 537 150 - 230 days ( $\phi_r$  between 62 - 95 days), indicating there is a steep drop off in optimized  
 538 response factors ( $\phi$ ) as beaches transition between a stable dissipative state ( $\bar{\Omega} \geq 6$ )  
 539 and the higher energy intermediate states ( $4 \leq \bar{\Omega} \leq 6$ ). The representative response  
 540 factors ( $\phi_r$ ) found in this study agree with previous results reported by *Hansen and*  
 541 *Barnard* [2010] at Ocean Beach, where a 90-day running mean of the offshore significant  
 542 wave height showed a similar cyclic pattern to the first two temporal modes of shoreline  
 543 variability.

544 Across all the exposed sites investigated here, the range of the rate parameter ( $c$ ;  
 545  $\text{m}^{1.5}\text{s}^{-1}\text{W}^{-0.5}$ ) varied by a factor of 2 between  $3.02 \times 10^{-8}$  at the most dissipative site  
 546 (North Head,  $\bar{\Omega} = 12.56$ ) and  $7.17 \times 10^{-8}$  (Ocean Beach,  $\bar{\Omega} = 5.26$ , Figure 3). The

erosion ratio ( $r$ ; eq. 4, Figure 3) also varied significantly between 0.23 (Truc Vert) and 0.45 (Gold Coast). Exploration of the dependency of these parameters ( $\phi$ ,  $c$ , and  $r$ ) on quantifiable environmental variables is discussed in more detail in Section 4.3. The linear trend term ( $b$ ; eq. 3, Figure 3) ranged from eroding at a rate of -4.52 m/yr (North Head) to accreting at a rate of 7.29 m/yr (OB8) and accounts for observed long-term trends in shoreline change not related to changes in wave height and period.

## 4.2. Semi-Embayed Coastlines

The semi-embayed sites at Narrabeen and Collaroy beaches consisted of five survey profiles and a sixth Argus-derived shoreline all obtained over the same 7-year period. The profile data is not alongshore averaged and therefore uncertainty associated with localized variability such as beach cusps and localized accretion/erosion are not accounted for.

At Narrabeen-Collaroy, storms occur throughout the year and the beach, which modally is classified as a rip-dominated beach, responds more rapidly to these changes in wave conditions via the rapid exchange of sediment between nearshore sandbars and the beach face [Davidson *et al.*, 2013]. The equilibrium model parameters are summarized in Figure 3. Model skill was ‘good’ (Table 4) at all six sites (Figure 5). Optimized response factors ( $\phi$ ) were 1-2 orders of magnitude lower than at the exposed open coastlines, ranging from 10 days at the most sheltered site (PF8), to the record mean ( $\geq 1000$  days) at the most exposed site (PF1). The shorter  $\phi$  values indicate the beach has a very short memory of past beach state conditions, while the more energetic northern end of the beach with a longer  $\phi$  value indicates the beach is oscillating around the annual mean wave condition. This alongshore variation of  $\phi$  as a function of wave exposure (i.e.  $\bar{\Omega}$ ) is expected based

568 on the timescales of sediment exchange between the beach face and the nearshore under  
569 reflective, intermediate and more dissipative conditions [*Wright et al.*, 1985].

570 Values of the rate parameter ( $c$ ; Figure 3) ranged from  $4.56 \times 10^{-8}$  at the most exposed  
571 semi-embayed site (PF1) to  $2.59 \times 10^{-7}$  at the most sheltered site considered here (PF8).  
572 While the more exposed site (PF1) had a  $c$  value which was mid-range to that found at the  
573 exposed coastlines, the variability among the semi-embayed sites was three times larger  
574 than the range observed at the exposed sites. However, the erosion ratio ( $r$ ) was relatively  
575 constant around the embayment and ranged between 0.40 and 0.46 (Figure 3). The linear  
576 trend term ( $b$ ), which captures the physical processes not presently encapsulated in the  
577 cross-shore equilibrium shoreline model ranged from -2.03 m/yr at the northern exposed  
578 end (PF1) to 2.05 m/yr at the southern end (PF6) indicating the embayment was most  
579 likely under-going a counter-clockwise rotation during this seven year period.

### 4.3. Inter-site Comparison of Model Coefficients

580 Eight sites (Figure 3 - 4) in this study were considered to be sufficiently skillful  
581 ( $R \geq 0.70$ , BSS  $\geq 0.6$ , NMSE  $\leq 0.4$ ) to examine if the (so far) site-specific wave-driven  
582 coefficients vary in a systematic manner across the broad spectrum of coastal settings  
583 represented in this study. Secondly, the goal is to determine if new parameterized forms  
584 can be simply derived from readily available environmental characteristics, such as local  
585 wave conditions and sediment grain size and therefore potentially reduce the need for  
586 extensive site-specific calibration data sets in the future.

#### 4.3.1. Wave-driven Model Coefficients

588 The two wave-driven model coefficients (refer to Section 3) that are optimized dur-  
589 ing the calibration process are  $\phi$  and  $c$ . The response factor ( $\phi$ ) describes the dominant

590 response time of cross-shore sediment exchange at a specific site, while the rate parameter ( $c$ ) represents the efficiency with which waves induce cross-shore sediment transport  
 591 resulting in onshore/offshore sandbar migration and shoreline change. Based on the dominant  
 592 nearshore morphology and sediment characteristics at each site, it is anticipated  
 593 that different types of beaches will respond differently to similar changes in wave conditions.  
 594 For example, it is commonly observed that energetic coastlines (higher  $\bar{\Omega}$ ), such  
 595 as North Head and Truc Vert, exhibit one or multiple offshore sandbars that effectively  
 596 dissipate incident band wave energy in the surf zone. Shoreline variability at these sites is  
 597 typically observed to respond at the timescales of the dominant seasonal variation in wave  
 598 climate (large  $\bar{\sigma}_{\Omega_{360}}/\bar{\sigma}_{\Omega_{30}}$ ), as sediment is cyclically transferred between offshore bars and  
 600 the beach face. Conversely, more sheltered coastlines (lower  $\bar{\Omega}$ ), such as Narrabeen and  
 601 Collaroy, tend to have more rhythmic nearshore sandbar features closer to the shoreline.  
 602 Sediment exchange between the subaerial beach and nearshore is typically more rapid. As  
 603 a result, shoreline variability tends to predominate at the storm time scale, rather than  
 604 the seasonal-scale.

605 Figure 6 shows the optimized filter values ( $\phi$ ) versus the weighted mean dimensionless  
 606 fall velocity ( $\bar{\Omega}_r$ , eq. 2) for all eight sites. It is observed that as  $\bar{\Omega}_r$  increases, so does  
 607 the response factor ( $\phi$ ), indicating that the shorelines along dissipative beaches tend to  
 608 respond to the seasonal changes in wave climate and are more resilient to individual  
 609 storms, while the shorelines of lower energy, more reflective beaches rapidly respond to  
 610 changes in wave energy. To synthesize these observations, a best-fit curve is shown in  
 611 Figure 6 using the weighted dimensionless fall velocity. The parameterized response factor  
 612 ( $\hat{\phi}$ ), where  $\hat{()}$  indicates a parameterized value is given by:

$$\hat{\phi} = \min[2 + \bar{\Omega}_r^2 + \exp(\bar{\Omega}_r - 4.65)^3, 1000], \quad (13)$$

613 where  $\exp$  represents the exponential function ( $e$ ). The parameterization  $\hat{\phi}$  fits the data  
 614 well ( $R^2 = 0.99$ , Figure 6) and can be usefully subdivided into three main categories  
 615 of shoreline response. When beaches are modally in the reflective state ( $\bar{\Omega}_r \leq 1$ ), the  
 616 response factor ( $\hat{\phi}$ ) is near constant. As  $\bar{\Omega}_r$  increases through the transitional/intermediate  
 617 beach states of bar-attached and bar-detached states,  $\hat{\phi}$  increases at a rate of  $\bar{\Omega}_r^2$  (Figure 6).  
 618 As the beach transitions into more dissipative states ( $\bar{\Omega}_r \geq 4.65$ ) there is an exponential  
 619 increase in  $\hat{\phi}$ . For highly dissipative beaches ( $\bar{\Omega}_r \geq 6$ ), the shoreline is again observed to  
 620 be more stable and the response factor ( $\hat{\phi}$ ) becomes independent of  $\bar{\Omega}_r$  and optimizes at  
 621 the order of 1000 days (i.e. several years) duration. A cutoff of 1000 days was selected  
 622 here as a practical upper bound of past data required, as this accounts for the past 2000  
 623 (i.e.  $2\phi$ ) days in calculating  $\Omega_{eq}$  (eq. 8). Further extending this upper bound does not  
 624 significantly alter  $\Omega_{eq}$  [Davidson *et al.*, 2013].

625 The rate parameter ( $c$ ) ranged from  $3.02 \times 10^{-8}$  at the most dissipative site (North  
 626 Head) to  $2.59 \times 10^{-7}$  at the most sheltered site (Collaroy, NBPF8), suggesting an inverse  
 627 relationship between  $c$  and mean offshore forcing ( $\bar{\Omega}$ ). Across all study sites, larger values  
 628 of the rate parameter ( $c$ ) were also associated with smaller values of the response factor  
 629 ( $\phi$ ) (Figure 3). As the present model formulation has a non-linear dependency between  
 630 these two terms, they are likely inter-dependent, however, the normalization of  $\Delta\Omega$  in (5)  
 631 by  $\sigma_{\Delta\Omega}$  limits this influence.

632 There are several physically-based explanations for this observed inverse relationship  
 633 of  $c$  and  $\bar{\Omega}$ . First is the physical shape of the profile of the beach. As  $\bar{\Omega}$  increases,



634 beaches tend to not only be located along coastlines exposed to higher waves, but also be  
 635 composed of finer sand (smaller  $d_{50}$ ) and exhibit milder nearshore beach slopes. By the  
 636 breakpoint hypothesis, a sandbar will develop at the cross-shore location of the depth-  
 637 limited breaking waves [e.g. *Dean, 1973*], and as such, on milder sloping beaches waves  
 638 break further offshore, resulting in wide surf zones that effectively dissipate wave energy  
 639 over the one to multiple sandbars that exist. This hypothesized efficiency to dissipate wave  
 640 energy further offshore results in less energy available to move sand onshore/offshore in  
 641 the nearshore and cause shoreline change. Conversely, on steeper, coarse sand beaches,  
 642 with smaller waves (low  $\bar{\Omega}$ ), the breaker line is closer to shore, inducing sediment transport  
 643 and the efficient and rapid exchange of sand between inshore sandbars and the beach face.  
 644 Also, beaches characterized by lower  $\bar{\Omega}$  are typically associated with more complex surf  
 645 zone morphology, while higher values of  $\bar{\Omega}$  typically are associated with alongshore linear  
 646 (multiple) sandbars [*Wright and Short, 1984*]. Complex surf zone morphology can induce  
 647 circulation that moves sediment onshore more efficiently than a linear system [*Splinter*  
 648 *et al., 2011a*], thus also increasing  $c$  for lower  $\bar{\Omega}$ .

649 The true explanation is likely to be a combination of the mechanisms mentioned above.  
 650 Curve fitting to the available data, a parameterized rate parameter ( $\hat{c}$ ) is derived:

$$\hat{c} = 3.05 \times 10^{-8} + (1.55 \times 10^{-6} \bar{\Omega}) e^{-\bar{\Omega}}. \quad (14)$$

651 This empirical relationship for  $\hat{c}$  ( $R^2 = 0.99$ , Figure 7) is consistent with the available  
 652 observations that for larger values of the mean dimensionless fall velocity associated  
 653 with dissipative beaches ( $\bar{\Omega} > 6$ ), the rate parameter converges to a constant value  
 654 ( $\hat{c} \rightarrow 3.01 \times 10^{-8}$ ). In contrast, during the transitional phases as the surf zone sand-

bars transition from bar-welded states to bar-detached states ( $1 \leq \bar{\Omega} \leq 6$ , Figure 7) there is an exponential decay in  $\hat{c}$  that is hypothesized to relate to the enhanced efficiency in cross-shore transport under complex surf-zone morphology. Albeit this empirically-derived parameterization fits the data quite well, the extension of the present curve beyond observations (particularly for  $\bar{\Omega} \leq 2$ ) should be taken with caution. Reflective beaches are generally less dynamic than intermediate beaches because they are nearly always coincident with lower energy levels ( $F$ , eq. 5) and coarser sediments (larger  $d_{50}$ ), which both inhibit the mobility of the shoreline (eq. 3). As such, as  $F \rightarrow 0$ ,  $dx/dt \rightarrow 0$  with no requirement that  $\hat{c} \rightarrow 0$  as well. However, allowing the parameterized rate parameter to exponentially increase as  $\bar{\Omega} \rightarrow 0$  would suggest reflective beaches are highly mobile, despite the usual coarse sand present. As such, new observations in this low energy reflective beach state are needed to confirm and/or refine this anticipated environmental dependency of  $\hat{c}$  for  $\bar{\Omega} \leq 2$ .

Significantly, the adoption of these two wave-driven parameterizations ( $\hat{\phi}$ : eq. 13 and  $\hat{c}$ : eq. 14) may provide the potential to utilize this equilibrium-based approach in predicting shoreline variability and change at a site based on local environmental variables (waves and sediments), rather than calibration to a pre-existing (or, more likely, non-existent) shoreline monitoring data set. An example of this approach is given in Section 5.2.

#### 4.3.2. The Erosion Ratio ( $r$ )

The erosion ratio defines the balance of the integrated accretion and erosion forcing (eq. 4) which would result in no trend in the shoreline for the optimized response factor ( $\phi$ ). While  $r$  is not a free parameter in the equilibrium model, large inter-site dependency was observed ( $0.23 \leq r \leq 0.46$ ) and therefore some further discussion is warranted. Similar to

678 the response factor and the rate parameter, the erosion ratio is likely to be influenced by  
 679 the efficiency of onshore transport and offshore bar morphology [*Splinter et al.*, 2011a],  
 680 whereby lower  $r$  values correspond to a system that is more resistant to erosion. Study  
 681 sites where the shoreline contour with respect to MSL ( $zRel$ , Table 2) was close to zero  
 682 (Gold Coast), had the highest  $r$  values ( $r = 0.45$ , Figure 3), while the larger tidal range  
 683 ( $\Delta Tide$ , Table 2) sites, which also utilized the MHW shoreline and were also the most  
 684 dissipative ( $\bar{\Omega} \geq 6$ ) sites available for inclusion in this work (Truc Vert ( $r = 0.23$ ) and  
 685 North Head ( $r = 0.30$ ) had some of the lowest  $r$  values. Based on curve-fitting to the  
 686 available data, a relationship to describe the erosion ratio is:

$$\hat{r} = 0.255 + \frac{1.32 - zRel}{\bar{\Omega}}. \quad (15)$$

687 The parameterization for  $\hat{r}$  ( $R^2 = 0.99$ , Figure 8) was the most complex of the three  
 688 parameterizations. The explicit inclusion of tidal range ( $\Delta Tide$ ) in (15) was also explored,  
 689 however, the additional complexity of  $\hat{r}$  for a small increase in model skill was not justified  
 690 for the data sets available here. However, for completeness the parameterized form for  $\hat{r}$   
 691 including tidal range is given ( $R^2 = 1.00$ ):

$$\hat{r} = 0.072(1 + \Delta Tide) + \frac{2.01 - 1.78zRel}{\bar{\Omega}}. \quad (16)$$

692 Similar to the parameterized form of the rate parameter ( $\hat{c}$ ), there was an inverse de-  
 693 pendence of the parameterized erosion ratio ( $\hat{r}$ ) on  $\bar{\Omega}$ . Like  $\hat{c}$ , it is hypothesized that this  
 694 is due to the varying efficiency of sand transfer between the beach face and the surf zone  
 695 sandbars. The shorelines of dissipative beaches (large  $\bar{\Omega}$ ) are resilient to small changes in  
 696 wave height as sand is predominantly moved during the slow cross-shore migration of off-

697 shore sandbars, while on more reflective/terrace beaches (small  $\bar{\Omega}$ ), more rapid exchanges  
698 of sediment between the beach face and the inshore sandbars dominate.

699 Similarly, (15) suggests that the parameterized erosion ratio decreases with increasing  
700 shoreline contour elevation ( $zRel$ ). Shoreline contours around MSL exhibit localized high  
701 variability, with potentially large horizontal excursions induced by minimal net sediment  
702 transport causing sandbars to weld and detach from the shoreline [e.g. *Castelle et al.*,  
703 2014]. In contrast, elevation contours higher up the beach face are less influenced by  
704 these small and rapid exchanges of sediment around MSL. This observation is likely more  
705 important on meso-macro tidal sites where significant quantities of sand can be trans-  
706 ported within the inter-tidal zone over a single tide cycle, resulting in a very ‘noisy’ MSL  
707 shoreline contour, as such, the MHW contour is preferred over the MSL contour when  
708 available [*Castelle et al.*, 2014].

## 5. Discussion

### 5.1. Equilibrium Shoreline Response

709 From the presentation above of data-model comparisons obtained across a broad spec-  
710 trum of sandy beach settings on three continents, it is evident that the equilibrium-based  
711 approach to model shoreline response was successful at capturing the seasonal to decadal-  
712 scale response of shorelines to time-varying wave conditions. As evidenced in Figures 4,  
713 5 and 9, the model did not capture the full magnitude of all the accretion and erosion  
714 events. These accretionary ‘spikes’ may be attributed to short-lived bar welding events,  
715 but some, including the 2008 event at Torrey Pines remain unexplained [*Yates et al.*,  
716 2009]. The under-estimation of erosion within the model during some events may be at-  
717 tributed to increased erosion due to large storm surge. A clear example of this is in the

718 mode results for Narrabeen mid-2007 (Figure 5). Wave heights during this East Coast  
719 Low exceeded 3 m for 65 hours, with a maximum recorded water level (tide and surge)  
720 of 0.365 m above mean sea level. The impact of high water levels, large setup due to the  
721 large waves and the storm lasting several tidal cycles resulted in significant dune erosion.  
722 The observed wave conditions, which are modeled in the disequilibrium term ( $\Delta\Omega$ ) along  
723 with the forcing ( $F$ ) were not enough to cause this magnitude of erosion in the model.  
724 While the model under-estimated erosion during this event, the model also did not pre-  
725 dict the magnitude of the rapid accretionary response of the shoreline post storm. Had  
726 the model predicted this magnitude of shoreline accretion post-storm the model and data  
727 would have potentially continued to diverge post mid-2007. Instead, the observed wave  
728 conditions produced a smaller disequilibrium and forcing in the model that resulted in  
729 only minor shoreline change over the next 2 - 3 months. This resulted in a modeled shore-  
730 line position of -5 m to -10 m below the record average (Figure 5), NB2600. When the  
731 observed shoreline eventually recovered from the storm and returned to being in relative  
732 equilibrium with the prevailing wave conditions, the model begins to track the data again  
733 by August 2007. This suggests that while the equilibrium model may not capture every  
734 event, the formulation is capable of self-correcting in time.

735 The equilibrium concept was most successful at the exposed open coastline sites ( $R \geq$   
736  $0.79$ ,  $BSS \geq 0.80$ ,  $NMSE \leq 0.4$ ; Table 4) where a change in wave steepness is anticipated  
737 to be the key driver in daily to seasonal shoreline variability. These open-coast sites are  
738 characterized by long response factors ( $\phi$ ), on the order of the seasonal to annual cycle  
739 (representative response factors,  $\phi_r = 62 - 414$  days), with changes in shoreline position  
740 and wave steepness well-correlated (Table 4).

741 The exception to this high model skill across all the exposed open coastlines available  
742 to this study was the model performance at the Duck, NC site. Previous analysis and ap-  
743 plication of an equilibrium shoreline model by *Miller and Dean* [2004a] at this same Duck  
744 site highlight how two adjacent stretches of coastline on either side of the pier can exhibit  
745 very different shoreline behavior. While the multi-year onshore and offshore movement of  
746 sandbars has been demonstrated to be well-correlated to changes in offshore wave height  
747 at the Duck site [e.g. *Plant et al.*, 1999], the results presented here are consistent with  
748 *Miller and Dean* [2004a]. As other researchers have reported, the lower model skill may be  
749 attributed to several complex processes influencing the shoreline at this Duck site. *Plant*  
750 *and Holman* [1996] previously observed that shoreline variability at the complex Duck site  
751 was dominated by rhythmic alongshore shoreline variability with length scales of order 1  
752 km that progressed at an average rate of 1m/day. While these features were modulated  
753 at a seasonal cycle, the alongshore averaged shoreline (as was used in this study) did not  
754 contain a significant annual cycle. *List et al.* [2006] also observed that shoreline change  
755 immediately adjacent (+/-5 km) to the FRF pier was quite small compared to the full  
756 Duck-Hatteras, NC cell, and that for this region of North Carolina, shoreline response  
757 was not significantly correlated to offshore peak wave height.

758 The equilibrium approach presented here performed well ( $0.61 \leq R \leq 0.82$ ; Table 4)  
759 at the semi-embayed beach sites for the period of survey data available here. As can  
760 be observed in Figure 5, the six survey sites around the Narrabeen-Collaroy embayment  
761 spanning the full range of higher to lower energy intermediate beach states indicate the  
762 embayment underwent a slight anti-clockwise rotation over the 7-year period of observa-  
763 tions. The northern profiles (PF1, PF2) exhibited a net erosive trend, while the southern

764 profiles (PF6, PF8) and alongshore averaged Argus-derived shoreline (NB2600) accreted  
765 during this period as indicted by the linear trend term ( $b$ , Figure 3). Contrary to initial  
766 expectations, the more sheltered (southern) end of the study embayment exhibited higher  
767 skill than the more exposed (northern) end. Two explanations for this range of skill are  
768 proposed. First, that the more sheltered end is less susceptible to longer-term (multi-year)  
769 rotational shifts in wave energy. Along the Australian East Coast it has been well docu-  
770 mented that semi-embayed coastlines, such as Narrabeen-Collaroy, adjust to this change  
771 in modal wave direction [*Ranasinghe et al.*, 2004], but the magnitude of change is less  
772 pronounced at the more sheltered ends [*Harley et al.*, 2011]. Second, shoreline response  
773 at the more sheltered ends of embayments along this stretch of coastline are primarily  
774 driven by the change in wave exposure due to the seasonal rotation between summer  
775 (more easterly) and winter (more southerly) waves as is observed in the seasonal variation  
776 of shorelines presented in Figure 5. Despite these regional-scale rotational effects, the  
777 equilibrium-based approach was still considered skillful ( $BSS \geq 0.7$  and  $NMSE \leq 0.6$ ;  
778 Table 4), supporting the concept that at the timescales of wave-driven cross-shore sedi-  
779 ment transport, the equilibrium concept driven by cross-shore processes predominantly  
780 controlled the shoreline position at all locations within the embayment. It is anticipated  
781 that the inclusion of an additional longshore component to this equilibrium-based ap-  
782 proach would likely assist by allowing the (sometimes contrasting) processes of longshore  
783 and cross-shore sediment transport to both contribute to the resulting shoreline response  
784 [*Harley et al.*, 2011; *van de Lageweg et al.*, 2013].

## 5.2. A Generalized Form of the Model

785 A robust model that can be reliably used and widely applied to predict shoreline vari-  
786 ability and change with minimal need for site-specific calibration is a sought after tool by  
787 coastal scientists and engineers alike. Here we test the performance of the equilibrium-  
788 based *ShoreFor* model (eq. 3) utilizing the new empirically-derived parameterizations for  
789 the wave-driven components presented above: the response factor ( $\hat{\phi}$ , eq. 13) and the rate  
790 parameter ( $\hat{c}$ , eq. 14). While the parameterization for the erosion ratio ( $\hat{r}$ , eq. 15) could  
791 also be included in (3), it is not a free parameter and is instead determined within the  
792 model to maintain the balance between onshore and offshore transport under equilibrium  
793 conditions. Forcing the parameterized erosion ratio ( $\hat{r}$ ) based on (15) does not necessarily  
794 change model skill, but can erroneously attribute model variance to the ‘unknown’ linear  
795 trend term ( $b$ ) rather than to temporal gradients in the wave forcing.

796 Comparing the skill assessment for both the site-specific calibration (Table 4) and the  
797 parameterized form of the model at the original 12 sites, four of which were not used in  
798 the parameterization, eight sites remained skillful ( $R \geq 0.7$ ; BSS  $\geq 0.6$ ; NMSE  $\leq 0.4$ ,  
799 Table 5). All 12 of the parameterized model results were defined as minimum ‘good’ based  
800 on BSS (Table 3) and five were ranked as ‘excellent’ (Table 5) similar to the results of  
801 the site-specific calibrated versions (Table 4). NMSE increased (or remained the same)  
802 at all sites, with eight sites being ranked as ‘good’ (Table 5) compared to eleven in  
803 the calibrated model results. Overall, the reduction of model coefficients by two is a  
804 significant improvement in the model with minimal loss of model skill, and therefore  
805 potentially increasing wider application of the equilibrium-based *ShoreFor* model at sites  
806 where insufficient data is available for calibration [refer to *Splinter et al.*, 2013a, b]. It is  
807 anticipated that the derived parameterizations, which were based on a minimum of five



808 years of data, could be used to predict shorelines for 5-10 year simulations [*Splinter et al.*,  
809 2013b], provided the wave climate was stationary (i.e.  $\bar{\Omega}$  did not vary significantly over  
810 the timescales of a model run). For longer term simulations, the ability for the response  
811 factor ( $\hat{\phi}$  eq. 13) and the rate parameter ( $\hat{c}$ , eq. 14), to adjust to changes in  $\bar{\Omega}$  and a  
812 time-varying linear trend term ( $b$ ) is expected to improve model performance and will be  
813 a topic of future research.

814 To further test the generalized model, we introduce an additional shoreline data set that  
815 was not used in the previous model assessment or free parameter derivation. Torrey Pines  
816 is a fine grained ( $d_{50} \sim 0.23$  mm), micro-tidal ( $\Delta\text{Tide} = 1.62$  m), sandy beach located at  
817 the southern end of an 82 km littoral cell in southern California [*Nordstrom and Inman*,  
818 1975]. Torrey Pines shoreline data has been used recently by several researchers to develop  
819 and test equilibrium-based shoreline models [*Miller and Dean*, 2004a; *Yates et al.*, 2009].  
820 The MSL shoreline positions over a 5 year period as presented in Figures 4 and 9 of *Yates*  
821 *et al.* [2009] were digitized and used here as a blind test case of an exposed beach that  
822 exhibits a strong seasonal signal in profile response related to changes in offshore wave  
823 conditions [e.g. *Aubrey*, 1979]. These digitized data were purposefully spaced at monthly  
824 intervals to avoid biasing correlation statistics for more closely sampled (weekly) surveys  
825 between May 2007 and May 2008 as is also presented in *Yates et al.* [2009].

826 Hourly wave data sourced from the deep water CDIP100 buoy was used to force the  
827 model, in place of the high resolution (100 m alongshore-spaced) spectral refraction wave  
828 model output at the -10 m contour directly offshore of Torrey Pines utilized in *Yates et al.*  
829 [2009], which was not available to the present study. This site is the least energetic of the  
830 exposed sites ( $\bar{\Omega} = 5.04$ ), but similar to the other sites has a large annual standard devi-

831 ation in waves ( $\bar{\sigma}_{\Omega_{360}} \sim 1.89$ ) that is observed in the annual cycle of shoreline variability.  
832 The ratio of  $\bar{\sigma}_{\Omega_{360}}/\bar{\sigma}_{\Omega_{30}} = 1.14$  and is comparable to Gold Coast, resulting in  $\bar{\Omega}_r = 5.75$ .  
833 Model skill utilizing the parameterized forms of  $\hat{\phi}$  (eq. 13) and  $\hat{c}$  (eq. 14) when applied  
834 to the digitized Torrey Pines shoreline data was ranked as ‘good’ to ‘excellent’ ( $R = 0.80$ ,  
835 BSS = 0.85, NMSE = 0.37, Table 5, Figure 9).

836 While the sites used here for empirically-derived versus site-specific model-model com-  
837 parison are quite diverse in their characteristics and the parameterized model showed good  
838 skill on a blind test site, many of the same observations underpin the two approaches.  
839 What is now required is to further test and likely refine the empirical formulations of  
840 the response factor ( $\hat{\phi}$ , eq. 13) and the rate parameter ( $\hat{c}$ , eq. 14) presented here, us-  
841 ing new survey data sets that may be available to other research teams. To assist this,  
842 a user-friendly (GUI-driven) version of the current *ShoreFor* model is available via the  
843 corresponding author.

## 6. Conclusions

844 Twelve shoreline data sets with suitable co-located wave data from a diverse range of  
845 beach sites were used to (1) calibrate and assess the generic applicability of the concept of  
846 wave-driven equilibrium shoreline response over timescales of weeks to a decade and (2)  
847 to further explore the dependence of the two wave-driven model coefficients on underlying  
848 environmental variables.

849 The concept of equilibrium-driven shoreline change was found to be most successful at  
850 exposed open coastlines, where a change in wave steepness is the predominant driving  
851 factor of shoreline change via onshore and offshore transport. The model reproduced the  
852 dominant seasonal cycle at five exposed sites with significant skill (BSS  $\geq 0.80$ , Table 4).

853 Semi-embayed beaches are more likely to be influenced by gradients in longshore transport,  
854 as well as cross-shore processes and therefore the application of wave-driven equilibrium  
855 shoreline models based on cross-shore processes only are time and site dependent.

856 Across the 12 sites the model coefficients were found to be systematically related to the  
857 dimensionless fall velocity ( $\Omega$ ). The response factor ( $\phi$ ) was found to be highly dependent  
858 on the mean ( $\bar{\Omega}$ ) and the mean standard deviation of  $\Omega$  at yearly ( $\bar{\sigma}_{\Omega_{360}}$ ) and monthly  
859 ( $\bar{\sigma}_{\Omega_{30}}$ ) timescales. The rate parameter ( $c$ ) was highly dependent on  $\bar{\Omega}$ . The empirical  
860 parameterizations for both terms ( $\hat{c}$ ,  $\hat{\phi}$ ) compared well with calibrated values ( $R^2 \geq 0.99$ )  
861 and were further utilized to test a generalized form of the model. The generalized form of  
862 the model remained skillful ( $BSS \geq 0.70$ ) at eight sites over the 5+ years of data available,  
863 plus one additional ‘blind’ test site that was not used in the initial analysis. While site-  
864 specific calibration is ideal, these new parameterizations can provide, at a minimum,  
865 initial estimates of model coefficients in methods such as those outlined in *Long and Plant*  
866 [2012], and perhaps also reducing the further need for extensive shoreline data sets to  
867 inform site-specific calibration.

868 **Acknowledgments.** This research was made possible with the help and data provided  
869 by many people, specifically the Argus user group who have provided the foundation and  
870 maintenance of numerous coastal imaging sites around the world. K.D.S. particularly  
871 wishes to thank R. Holman and J. Stanley of the Coastal Imaging Lab (CIL, Oregon  
872 State University) for their continued support in all things Argus and for always pushing  
873 her to think harder. The CIL is funded in part by the Office of Naval Research, N00014-  
874 10-1-0046. Argus-derived shoreline data from North Head, WA, USA was supplied by  
875 NWRA with funding from USACE Portland District. Gold Coast and Narrabeen Argus-

876 derived shorelines were provided by the UNSW Australia, Water Research Laboratory  
877 in partnership with Warringah Council and Gold Coast City Council. Profile data from  
878 Duck, NC were obtained from the U.S. Army Corps of Engineers Field Research Facility  
879 (FRF). Beach Surveys at Truc Vert were funded by SOLAQUI and Region Aquitaine.  
880 K.D.S. wishes to thank J.K. Miller for providing historical data for Torrey Pines and  
881 Duck in the initial stages of this work. Wave data was obtained from Manly Hydraulics  
882 Laboratory, Gold Coast City Council, the FRF, NOAA & CDIP buoys, WWIII (Truc  
883 Vert) and SWAN modeling from E. Kearney and J. Hansen (USGS). Funding for K.D.S.  
884 was provided under ARC Linkage project LP100200348 with support from NSW Office of  
885 Environment and Heritage, Warringah Council and CoastalCOMS. M.A.D. would like to  
886 thank the Plymouth Universities' Marine Institute for financial support for his sabbatical  
887 that made this work possible and a special thanks to UNSW Australia, School of Civil and  
888 Environmental Engineering for funding and hosting his visits to work with the Australian  
889 team. B.C. is funded by project BARBEC (ANR N2010 JCJC 60201). The GUI was  
890 developed by T. Beuzen under the direction of K.D.S. and I.L.T and funded by a UNSW  
891 Australia, School of Civil & Environmental Engineering Elite Student Scholarship.

## References

- 892 Alexander, P. S., and R. A. Holman (2004), Quantitative analysis of nearshore morpho-  
893 logical variability based on video imaging, *Marine Geology*, 208(1), 101–111.
- 894 Allen, M., and J. Callaghan (1999), Extreme wave conditions for the South Queensland  
895 coastal region, *Report*, EPA Queensland.

- 896 Anderson, T. R., L. N. Frazer, and C. H. Fletcher (2010), Transient and persis-  
897 tent shoreline change from a storm, *Geophysical Research Letters*, *37*, L08,401, doi:  
898 10.1029/2009GL042252.
- 899 Aubrey, D. G. (1979), Seasonal patterns of onshore/offshore sediment movement, *Journal*  
900 *of Geophysical Research*, *84*, 6347–6354.
- 901 Barnard, P., J. E. Hansen, and L. H. Erikson (2012), Synthesis study of an erosion hot  
902 spot, Ocean Beach, California, *Journal of Coastal Research*, *28(4)*, 903–922.
- 903 Birkemeier, W. A., H. C. Miller, S. D. Wilhelm, A. E. DeWall, and C. S. Gorbics (1985),  
904 User’s guide to CERC’s Field Research Facility, *Tech. Rep. Instruction Report-85-1*,  
905 Coastal Eng. Res. Cent., Field Res. Fac., U. S. Army Eng. Waterw. Exp. Sta., Vicksburg,  
906 Miss.
- 907 Callaghan, D. P., P. Nielsen, A. Short, and R. Ra (2008), Statistical simulation of wave  
908 climate and extreme beach erosion, *Coastal Engineer*, *55*, 375–390.
- 909 Carley, J. T., I. L. Turner, E. D. Couriel, L. A. Jackson, and J. E. McGrath (1999),  
910 The practical application of four commercially available numerical beach morphology  
911 models on a high energy coastline, in *Proceedings of the Australian Coastal and Ocean*  
912 *Engineering Conference*, pp. 101–106, Perth, AU.
- 913 Castelle, B., P. Bonneton, H. Dupuis, and N. Senechal (2007a), Double bar beach dy-  
914 namics on the high-energy meso-marcotidal French Aquatian Coast: a review, *Marine*  
915 *Geology*, *245*, 141–159.
- 916 Castelle, B., I. Turner, B. G. Ruessink, and R. Tomlinson (2007b), Impact of storms on  
917 beach erosion: Broadbeach (Gold Coast, Australia), *Journal of Coastal Research*, *SI*  
918 *50*, 534–539.

- 919 Castelle, B., V. Marieu, S. Bujan, S. Ferreira, J.-P. Parisot, S. Capo, N. Senechal,  
920 and T. Chouzenoux (2014), Equilibrium shoreline modelling of a high-energy meso-  
921 macrotidal multiple-barred beach, *Marine Geology*, *347*, 84–94.
- 922 Clarke, D., and I. Eliot (1988), Low-frequency changes of sediment volume on the beach-  
923 face at Warilla Beach, New South Wales, 1975–1985, *Marine Geology*, *79*, 189 – 211,  
924 doi:10.1016/0025-3227(88)90039-4.
- 925 Davidson, M., I. Turner, and R. Guza (2011), The effect of temporal wave averaging on  
926 the performance of an empirical shoreline evolution model, *Coastal Engineering*, *58*,  
927 802–805.
- 928 Davidson, M. A., and I. L. Turner (2009), A behavioral template beach profile model for  
929 predicting seasonal to interannual shoreline evolution, *Journal of Geophysical Research*,  
930 *114*, F01,020, doi:10.1029/2007JF000888.
- 931 Davidson, M. A., R. P. Lewis, and I. L. Turner (2010), Forecasting seasonal to multi-year  
932 shoreline change, *Coastal Engineering*, *57*, 620–629, doi:10.1016/j.coastaleng.2010.02.  
933 001.
- 934 Davidson, M. A., K. D. Splinter, and I. L. Turner (2013), A simple equilibrium model for  
935 predicting shoreline change, *Coastal Engineering*, *73*, 191–202, doi:10.1016/j.coastaleng.  
936 2012.11.002.
- 937 Dean, R. G. (1973), Heuristic models of sand transport in the surf zone, in *Proc. of the*  
938 *1st Australian Cong. on Coastal Eng., Conference on Engineering Dynamics in the Surf*  
939 *Zone*, pp. 209–214, Sydney, Australia.
- 940 Delft (1970), Gold Coast, Queensland, Australia - coastal erosion and related problems.,  
941 *Tech. Rep. R257*, Delft Hydraulics Laboratory.

- 942 Eshleman, J. L., P. L. Barnard, L. H. Erikson, and D. M. Hanes (2007), Coupling along-  
943 shore variations in wave energy to beach morphologic change using the SWAN wave  
944 model at Ocean Beach, San Francisco, CA., in *10th International Workshop on Wave  
945 Hindcasting and Forecasting and Coastal Hazard Symposium*, p. 20p, North Shore, Oahu,  
946 Hawaii, USA.
- 947 Frazer, L. N., T. R. Anderson, and C. H. Fletcher (2009), Modeling storms improves  
948 estimates of long-term shoreline change, *Geophysical Research Letters*, *36*, L20,404, doi:  
949 10.1029/2009GL040061.
- 950 Hansen, J., E. Elias, and P. Barnard (2013a), Changes in surf zone morphodynamics driven  
951 by multi-decadal contraction of a large ebb-tidal delta, *Marine Geology, Special Issue  
952 San Francisco Bay, 345*, 221–234, doi:<http://dx.doi.org/10.1016/j.margeo.2013.07.005>.
- 953 Hansen, J., E. Elias, J. List, L. Erikson, and P. Barnard (2013b), Tidally influenced  
954 alongshore circulation at an inlet-adjacent shoreline, *Continental Shelf Research*, *56*,  
955 26–38, doi:[10.1016/j.csr.2013.01.017](http://dx.doi.org/10.1016/j.csr.2013.01.017).
- 956 Hansen, J. E., and P. L. Barnard (2010), Sub-weekly to interannual variability of a high-  
957 energy shoreline, *Coastal Engineering*, *57*, 959–972, doi:[10.1016/j.coastaleng.2010.05.](http://dx.doi.org/10.1016/j.coastaleng.2010.05.011)  
958 011.
- 959 Hanson, H., and N. Kraus (1989), Generalized model for simulating shoreline  
960 change, Report 1, Technical Reference, *Tech. rep.*, U.S. Army Engineer Waterways Ex-  
961 periment Station; Coastal Engineering Research Center (U.S.); United States. Army.  
962 Corps of Engineers.
- 963 Harley, M. D., I. L. Turner, A. D. Short, and R. Ranasinghe (2011), A re-evaluation of  
964 coastal embayment rotation: the dominance of cross-shore versus alongshore sediment

- 965 transport processes, Collaroy-Narrabeen Beach, SE Australia, *Journal of Geophysical*  
966 *Research*, *116*, F04,033, doi:10.1029/2011JF001989.
- 967 Holman, R., J. Stanley, and H. Özkan Haller (2003), Applying video sensor networks to  
968 nearshore environmental monitoring, *IEEE Pervasive Computing*, *2*(4), 14–21.
- 969 Idier, D., B. Castelle, E. Charles, and C. Mallet (2013), Longshore sediment flux hindcast:  
970 spatio-temporal variability along the SW Atlantic coast of France, *Journal of Coastal*  
971 *Research*, *Si 65*, 17851790.
- 972 Karunarathna, H., and D. E. Reeve (2013), A model for beach plan shape change using  
973 an inverse approach, in *Coastal Dynamics 2013*, pp. 937–946.
- 974 Komar, P. D. (1974), *Beach Processes and Sedimentation*, Prentice-Hall, Englewood Cliffs,  
975 N.J.
- 976 Larson, M., and N. Kraus (1989), SBEACH: Numerical model for simulating storm-  
977 induced beach change; Report 1, Empirical foundation and model development, *Tech.*  
978 *Rep. CERC 89-9*, Coastal Engineering Research Center.
- 979 Lippmann, T., and R. Holman (1990), The spatial and temporal variability of sand bar  
980 morphology, *Journal of Geophysical Research*, *95*(C7), 11,575–11,590.
- 981 List, J. H., A. S. Farris, and C. Sullivan (2006), Reversing storm hotspots on sandy  
982 beaches: Spatial and temporal characteristics, *Marine Geology*, *226*, 261–279.
- 983 Long, J. W., and N. G. Plant (2012), Extended kalman filter framework for fore-  
984 casting shoreline evolution, *Geophysical Research Letters*, *39*(L13603), doi:10.1029/  
985 2012GL052180.
- 986 McCall, R., J. Van Thiel de Vries, N. Plant, A. Van Dongeren, J. Roelvink, D. Thompson,  
987 and A. Reniers (2010), Two-dimensional time dependent hurricane overwash and erosion



- 988 modeling at Santa Rosa Island, *Coastal En*, 57, 668–683.
- 989 Miller, J. K., and R. G. Dean (2003), Implications of longshore variability in shoreline  
990 change modeling, in *Proceedings of Coastal Sediments 2003*, pp. 1–14, World Scientific  
991 and East Meets West Productions, Corpus Christi, TX.
- 992 Miller, J. K., and R. G. Dean (2004a), A simple new shoreline change model, *Coastal*  
993 *Engineering*, 51, 531–556.
- 994 Miller, J. K., and R. G. Dean (2004b), A simple new shoreline evolution model, in *Pro-*  
995 *ceedings of the 29th International Conference on Coastal Engineering*, vol. 2, edited by  
996 J. M. Smith, pp. 2009–2021, ASCE, World Scientific.
- 997 Nordstrom, C. E., and D. L. Inman (1975), Sand level changes on Torrey Pines Beach,  
998 California., *MP 11-75*, U. S. Army Corps Engineers, Coastal Engineering Research  
999 Center.
- 1000 Patterson, D. (2007), Sand transport and shoreline evolution, Northern Gold Coast, Aus-  
1001 tralia, in *Proceedings of the 9th International Coastal Symposium*, pp. 147–151, Journal  
1002 of Coastal Research SI 50.
- 1003 Pelnard-Considere, R. (1956), Essai de theorie do l’evolution des forms de ravage en plage  
1004 de sable et de galets, *4me Journees de l’Hydraulique, Les Energies de la Mer, Question*  
1005 *III*(Rapport No. 1), 289–298.
- 1006 Pender, D., and H. Karunarathna (2013), A statistical-process based approach for mod-  
1007 elling beach profile variability, *Coastal Engineering*, 81(0), 19 – 29, doi:[http://dx.doi.](http://dx.doi.org/10.1016/j.coastaleng.2013.06.006)  
1008 [org/10.1016/j.coastaleng.2013.06.006](http://dx.doi.org/10.1016/j.coastaleng.2013.06.006).
- 1009 Plant, N., R. Holman, and M. Freilich (1999), A simple model for interannual sand bar  
1010 behavior, *Journal of Geophysical Research*, 104(C7), 15,755–15,776.

- 1011 Plant, N. G., and R. A. Holman (1996), Interannual shoreline variations at Duck, NC,  
1012 USA, in *Proceedings of the 25th International Conference On Coastal Engineering*, pp.  
1013 3521–3533, ASCE, Orlando, FL.
- 1014 Ranasinghe, R., R. McLoughlin, A. Short, and G. Symonds (2004), The Southern Os-  
1015 cillation Index, wave climate, and beach rotation, *Marine Geology*, *204*, 273–287, doi:  
1016 10.1016/S0025-3227(04)00002-7.
- 1017 Roelvink, D., A. Reniers, A. van Dongeren, J. van Thiel de Vries, R. McCall, and J. Lescin-  
1018 ski (2009), Modelling storm impacts on beaches, dunes and barrier islands, *Coastal*  
1019 *Engineering*, *56*(11-12), 1133 – 1152, doi:10.1016/j.coastaleng.2009.08.006.
- 1020 Ruessink, B., L. Pape, and I. Turner (2009), Daily to interannual cross-shore sandbar  
1021 migration: observations from a multiple sandbar system, *Continental Shelf Research*,  
1022 *29*, 1663–1677.
- 1023 Ruggiero, P., D. Walstra, G. Gelfenbaum, and M. van Ormondt (2009), Seasonal-scale  
1024 nearshore morphological evolution: Field observations and numerical modeling, *Coastal*  
1025 *Engineering*, *56*(1112), 1153 – 1172, doi:http://dx.doi.org/10.1016/j.coastaleng.2009.  
1026 08.003.
- 1027 Ruggiero, P., M. Buijsman, G. M. Kaminsky, and G. Gelfenbaum (2010), Modeling the  
1028 effects of wave climate and sediment supply variability on large-scale shoreline change,  
1029 *Marine Geology*, *273*(1-4), 127 – 140, doi:DOI:10.1016/j.margeo.2010.02.008.
- 1030 Senechal, N., T. Gouriou, B. Castelle, J.-P. Parisot, S. Capo, S. Bujan, and H. Howa  
1031 (2009), Morphodynamic response of a meso- to macro-tidal intermediate beach based  
1032 on a long-term data set, *Geomorphology*, *107*, 263–274.

- 1033 Short, A. D., and A. C. Trembanis (2004), Decadal scale patterns in beach oscillation and  
1034 rotation Narrabeen Beach, Australia - time series, PCA, and wavelet analysis, *Journal*  
1035 *of Coastal Research*, *20*(2), 523–532.
- 1036 Splinter, K. D., and M. L. Palmsten (2012), Modeling dune response to an East Coast Low,  
1037 *Marine Geology*, *329-331*, 46–57, doi:http://dx.doi.org/10.1016/j.margeo.2012.09.005.
- 1038 Splinter, K. D., R. Holman, and N. Plant (2011a), A behavior-oriented dynamic model for  
1039 sand bar migration and 2DH evolution, *Journal of Geophysical Research*, *116*, C01,020,  
1040 doi:10.1029/2010JC006382.
- 1041 Splinter, K. D., D. Strauss, and R. Tomlinson (2011b), Assessment of post-storm re-  
1042 covery of beaches using video imaging techniques: A case study at Gold Coast, Aus-  
1043 tralia, *IEEE Transactions on Geoscience and Remote Sensing*, *49*(12), 4704–4716, doi:  
1044 10.1109/TGRS.2011.2136351.
- 1045 Splinter, K. D., M. A. Davidson, A. Golshani, and R. B. Tomlinson (2012), Climate  
1046 controls on longshore sediment transport, *Continental Shelf Research*, *48*, 146–156, doi:  
1047 10.1016/j.csr.2012.07.018.
- 1048 Splinter, K. D., M. A. Davidson, and I. L. Turner (2013a), Monitoring data requirements  
1049 for shoreline prediction: How much, how long, how often, in *Proceedings of the 12th*  
1050 *International Coastal Symposium (Plymouth England)*, *Journal of Coastal Research*,  
1051 *SI 65*, edited by D. C. Conley, G. Masselink, P. E. Russell, and T. J. O’Hare, pp.  
1052 2179–2184.
- 1053 Splinter, K. D., I. L. Turner, and M. A. Davidson (2013b), How much data is enough? The  
1054 importance of morphological sampling interval and duration for calibration of empirical  
1055 shoreline models, *Coastal Engineering*, *77*, 14–27, doi:10.1016/j.coastaleng.2013.02.009.

- 1056 Splinter, K. D., J. T. Carley, A. Golshani, and R. Tomlinson (2014), A relationship to  
1057 describe the cumulative impact of storm clusters on beach erosion, *Coastal Engineering*,  
1058 *83*(0), 49 – 55, doi:http://dx.doi.org/10.1016/j.coastaleng.2013.10.001.
- 1059 Sutherland, J., and R. L. Soulsby (2003), Use of model performance statistics in modelling  
1060 coastal morphodynamics., in *Proceedings of Coastal Sediments '03*, vol. CD-ROM, pp.  
1061 1–14, World Scientific Publishing Co.
- 1062 van de Lageweg, W., K. Bryan, G. Coco, and B. Ruessink (2013), Observations of  
1063 shoreline-sandbar coupling on an embayed beach, *Marine Geology*, *344*(0), 101 – 114,  
1064 doi:http://dx.doi.org/10.1016/j.margeo.2013.07.018.
- 1065 van Enckevort, I., B. Ruessink, G. Coco, K. Suzuki, I. Turner, N. Plant, and R. A. Holman  
1066 (2004), Observations of nearshore crescentic sandbars, *Journal of Geophysical Research*,  
1067 *109*, C06,028, doi:10.1029/2003JC002214.
- 1068 van Rooijen, A., A. Reniers, J. van Thiel de Vries, C. Blenkinsopp, and R. McCall (2012),  
1069 Modeling swash zone sediment transport at Truc Vert Beach, in *Proceedings of the*  
1070 *33rd Conference on Coastal Engineering*, edited by P. Lynett and J. M. Smith, ASCE,  
1071 Santander, Spain.
- 1072 Wright, L. D., and A. D. Short (1984), Morphodynamic variability of surf zones and  
1073 beaches: A synthesis, *Marine Geology*, *56*, 93–118.
- 1074 Wright, L. D., A. D. Short, and M. O. Green (1985), Short-term changes in the mor-  
1075 phodynamic states of beaches and surf zones: An empirical predictive model, *Marine*  
1076 *Geology*, *62*, 339–364.
- 1077 Yates, M. L., R. T. Guza, and W. C. O'Reilly (2009), Equilibrium shoreline response:  
1078 Observations and modeling, *Journal of Geophysical Research*, *114*, C09,014, doi:10.

1079 1029/2009JC005359.

1080 Yates, M. L., R. T. Guza, W. C. O'Reilly, J. E. Hansen, and P. L. Barnard (2011),

1081 Equilibrium shoreline response of a high wave energy beach, *Journal of Geophysical*

1082 *Research*, 116, C04,014, doi:10.1029/2010JC006681.

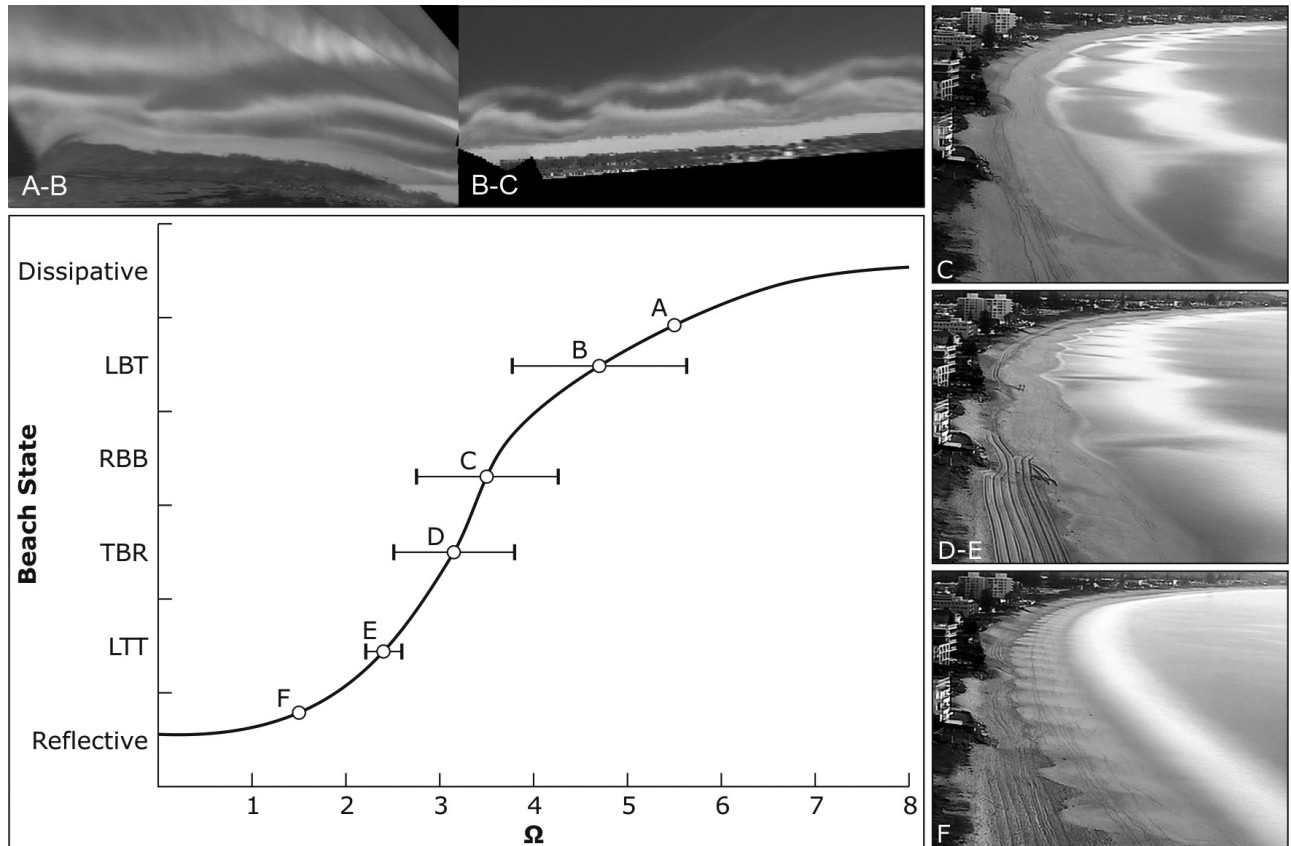


**Figure 1.** Example beach states with respect to dimensionless fall velocity as described in *Wright and Short* [1984]. A-B) dissipative at North Head, Washington; B-C) longshore bar - trough (LBT) and rhythmic bar - beach (RBB) at Gold Coast, Queensland; C) RBB; D-E) transverse - bar - rip (TBR) and low-tide terrace (LTT); F) reflective. C-F are from Narrabeen, New South Wales

**Table 1.** Summary of site statistics. <sup>a</sup> sediment grain size varies considerably at these sites. Previously reported values/means are used here.

Site	Type	$d_{50}$ (mm)	$\bar{\Omega}$	$\bar{\sigma}_{\Omega_{360}}$	$\bar{\sigma}_{\Omega_{30}}$	$\bar{\sigma}_{\Omega_{360}}/\bar{\sigma}_{\Omega_{30}}$	Primary Wave Buoy ID (depth, m)
North Head, WA	Exposed	0.2	12.38	4.48	3.69	1.21	NDBC 46029 (145)
Truc Vert, FR	Exposed	0.3 <sup>a</sup>	6.19	2.70	2.22	1.22	WWIII(70) & Buoy (54m)
Gold Coast, QLD	Exposed	0.25	6.17	2.08	1.84	1.13	Gold Coast (17)
Ocean Beach, OB8, CA	Exposed	0.3	5.29	1.78	1.50	1.19	CDIP 029 (550) & SWAN (10)
Ocean Beach, OB5, CA	Exposed	0.3	5.21	1.73	1.48	1.17	
Torrey Pines, CA	Exposed	0.23	5.04	1.89	1.65	1.12	CDIP 100 (554)
Duck, NC	Exposed	0.3 <sup>a</sup>	5.06	2.61	2.35	1.11	FRF (17)
Narrabeen, PF1, NSW	Embayed	0.4	4.08	1.36	1.27	1.07	
Narrabeen, PF2, NSW	Embayed	0.4	3.73	1.25	1.17	1.08	
Narrabeen, PF4, NSW	Embayed	0.4	3.75	1.32	1.23	1.07	Sydney (74) & SWAN (15)
Narrabeen, PF6, NSW	Embayed	0.4	3.67	1.31	1.23	1.07	
Narrabeen, PF8, NSW	Embayed	0.4	3.08	1.23	1.15	1.07	
Narrabeen, 2600, NSW	Embayed	0.4	3.67	1.31	1.23	1.07	

**Table 2.** Summary of survey data and wave sources. <sup>a</sup> Gold Coast is derived from the Argus Timex image closest to MSL. Using an average wave height of 1.2 m, setup is roughly 0.2 m. <sup>b</sup> Data from Torrey Pines was digitized from Figures 4 and 9 of *Yates et al.* [2009] at roughly monthly intervals. Where the shoreline was interpolated from a surface, estimated uncertainty was taken as 2 m, whereas if the shoreline was extracted from a single image or from a profile, the uncertainty was taken as 5 m.

Site	Date Range	Number of Surveys	Alongshore Average (m)	Type	Estimated Uncertainty in measurement (m)	Frequency	Shoreline Contour wrt MSL ( $z_{Rel}$ , m)	Mean Spring Tidal range ( $\Delta T_{ide}$ , m)
North Head, WA	2006-12	176	1000	Argus	2	bi-weekly	MHW (0.81)	2.3
Truc Vert, FR	2005-13	121	350-1200	Survey	2	monthly	MHW (1.5)	3.7
Gold Coast, QLD	2001-08	329	1000	Argus	5	weekly	MSL (0.2 <sup>a</sup> )	1.5
Ocean Beach, CA	2004-13	110-114	500	Survey	2	monthly	MHW (0.64)	1.83
Torrey Pines, CA	2003-09	80	-	Profile <sup>b</sup>	5	monthly	MSL (0)	1.62
Duck, NC	2000-06	58	230	Profile	2	monthly	MHW (0.65)	1.2
Narrabeen, NSW	2005-12	94	-	Profile	5	monthly	MHW (0.7)	2
Narrabeen, NSW	2005-12	434	400	Argus	2	weekly	MHW (0.7)	2



**Table 3.** Summary of qualitative skill assessments based on Brier Skill Scores (BSS) and normalized mean square error (NMSE).

Skill	BSS	NMSE
Poor	0 - 0.3	> 0.8
Fair	0.3 - 0.6	0.6- 0.8
Good	0.6 - 0.8	0.3 - 0.6
Excellent	> 0.8	< 0.3

**Table 4.** Skill assessment of all model results based on individual calibration to full data set.

Significant skill is defined as having an  $R \geq 0.70$  and BSS  $\geq 0.6$ .

Site	$R$	BSS	NMSE	Significant
North Head, WA	0.82	0.85	0.33	Y
Truc Vert, FR	0.83	0.83	0.31	Y
Gold Coast, QLD	0.80	0.80	0.36	Y
Ocean Beach, OB8, CA	0.80	0.80	0.40	Y
Ocean Beach, OB5, CA	0.79	0.81	0.37	Y
Duck, NC	0.72	0.68	0.48	N
Narrabeen, PF1, NSW	0.65	0.72	0.58	N
Narrabeen, PF2, NSW	0.61	0.72	0.63	N
Narrabeen, PF4, NSW	0.63	0.76	0.60	N
Narrabeen, PF6, NSW	0.81	0.76	0.35	Y
Narrabeen, PF8, NSW	0.78	0.70	0.39	Y
Narrabeen, 2600, NSW	0.82	0.78	0.33	Y

**Table 5.** Skill assessment of all model results based on parameterized model ( $c$  and  $\phi$ ).

Significant skill is defined as having an  $R \geq 0.70$  and BSS  $\geq 0.6$ .

Site	$R$	BSS	NMSE	Significant
North Head, WA	0.82	0.85	0.33	Y
Truc Vert, FR	0.83	0.84	0.32	Y
Gold Coast, QLD	0.80	0.80	0.36	Y
Ocean Beach, OB8, CA	0.80	0.81	0.37	Y
Ocean Beach, OB5, CA	0.71	0.80	0.51	Y
Duck, NC	0.63	0.61	0.66	N
Narrabeen, PF1, NSW	0.59	0.68	0.67	N
Narrabeen, PF2, NSW	0.57	0.69	0.74	N
Narrabeen, PF4, NSW	0.55	0.68	0.71	N
Narrabeen, PF6, NSW	0.80	0.74	0.36	Y
Narrabeen, PF8, NSW	0.78	0.69	0.40	Y
Narrabeen, 2600, NSW	0.82	0.76	0.34	Y
Torrey Pines, CA	0.80	0.85	0.37	Y



**Figure 2.** Map of the seven geographic locations encompassing the 13 transects/sites used in the present paper.

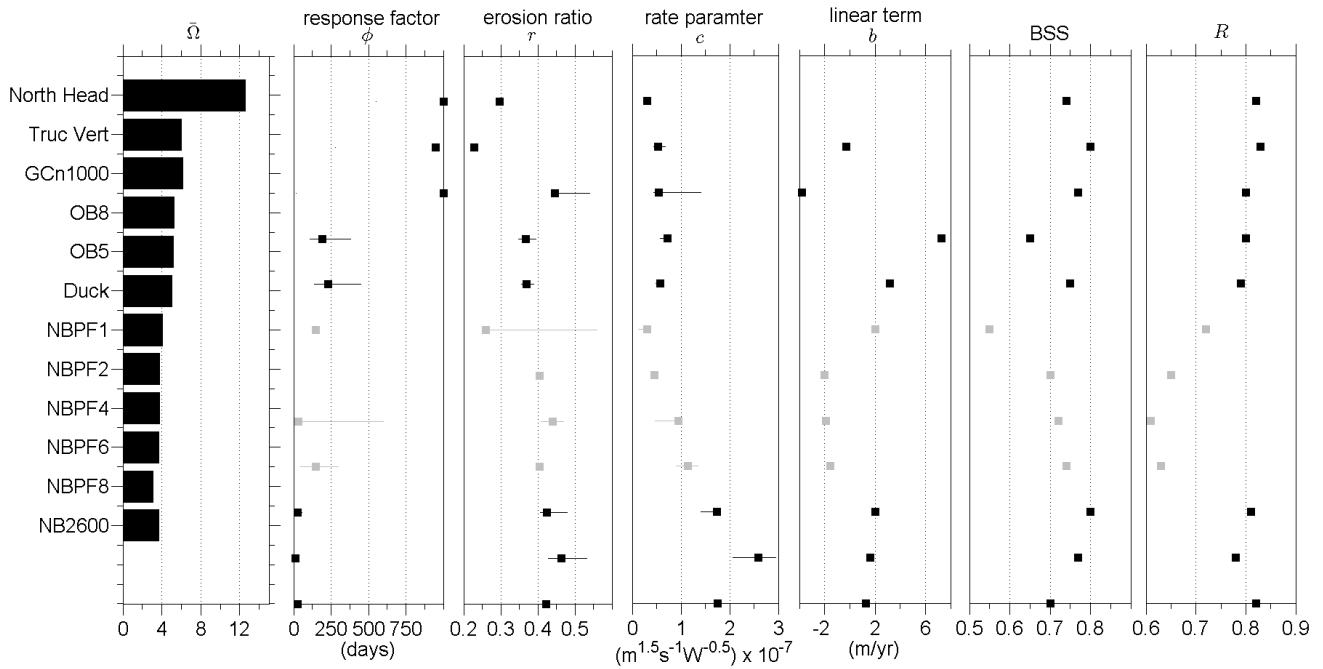


**Figure 3.** Summary statistics from all model runs. Grey indicates model skill is not considered significant enough to be included in further analysis. Significance is defined here as having an  $R \geq 0.70$  and a  $BSS \geq 0.6$ . Horizontal lines indicate the range of coefficient values where  $R^2$  did not decrease by more than 10% of maximum. Panels left to right: Mean dimensionless fall velocity ( $\bar{\Omega}$ ); response factor ( $\phi$ ); erosion ratio ( $r$ ); rate parameter ( $c$ ); linear term ( $b$ ); model Brier Skills Score (BSS); and model Correlation ( $R$ ).

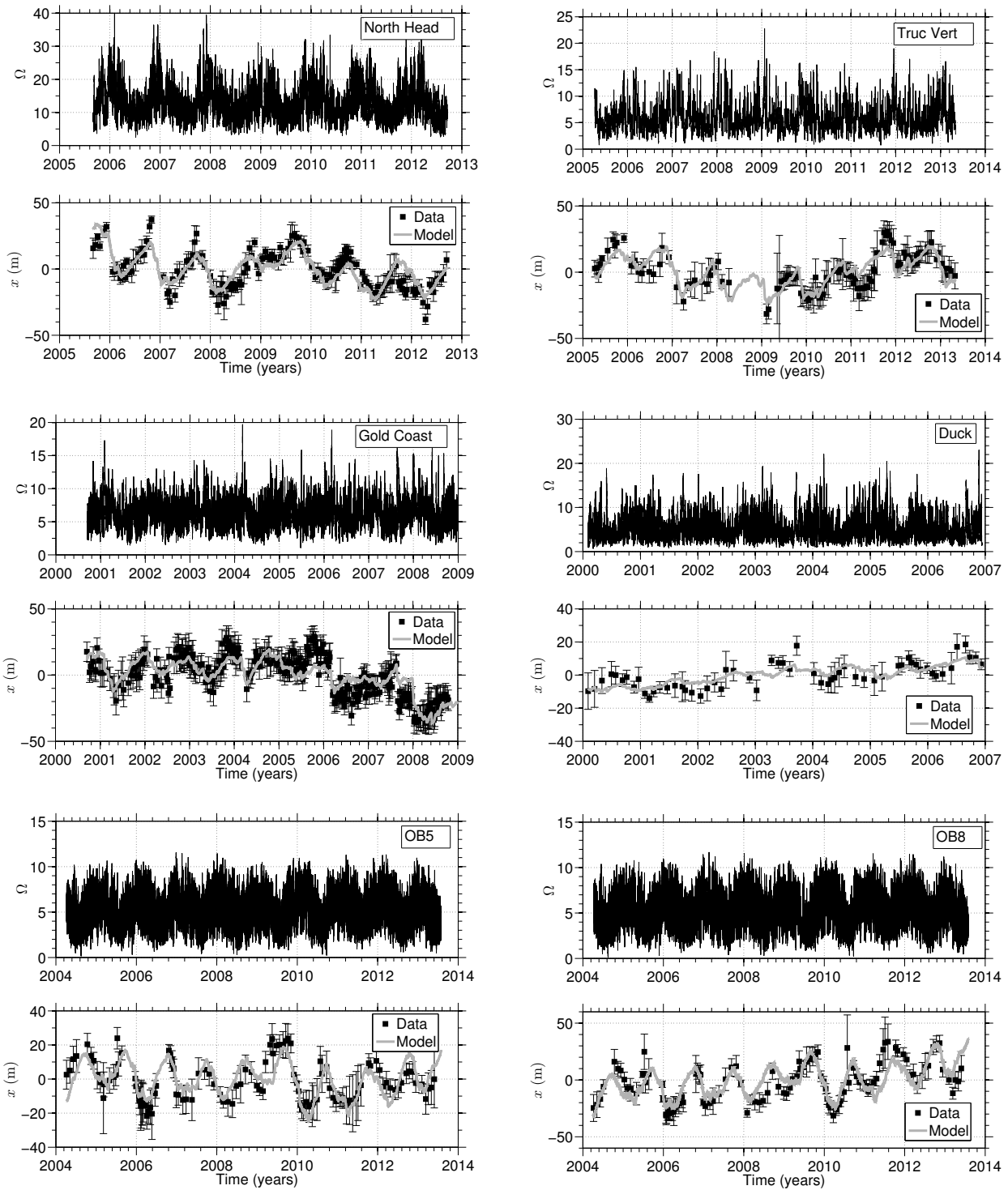


**Figure 4.** Equilibrium shoreline response for exposed, open-beaches. Subfigures are labelled by individual site and in each the following applies: the top plot shows the time series of dimensionless fall velocity; the bottom plot shows the observed shoreline data with the mean removed (solid black square with error bars representing both the uncertainty in the measurement technique, and where available, the time varying alongshore standard deviation of the mean shoreline as described in Table 2) and the model prediction (solid grey line).

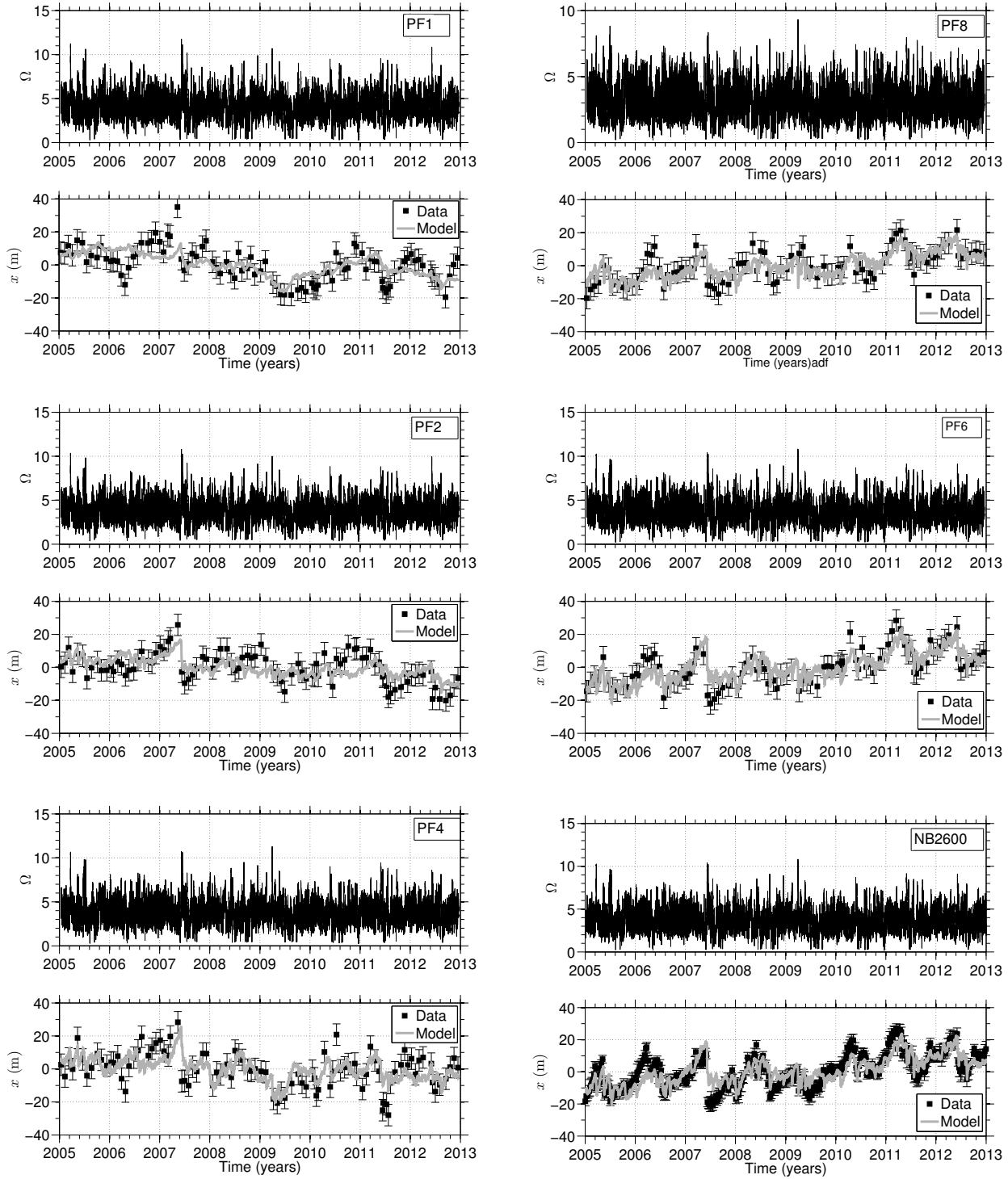


**Figure 5.** Equilibrium shoreline response for semi-embayed coastlines. Subfigures are labelled by individual site and in each the following applies: the top plot shows the time series of dimensionless fall velocity; the bottom plot shows the observed shoreline data with the mean removed (solid black square with error bars representing both the uncertainty in the measurement technique, and where available, the alongshore standard deviation of the mean shoreline as described in Table 2) and the model prediction (solid grey line).

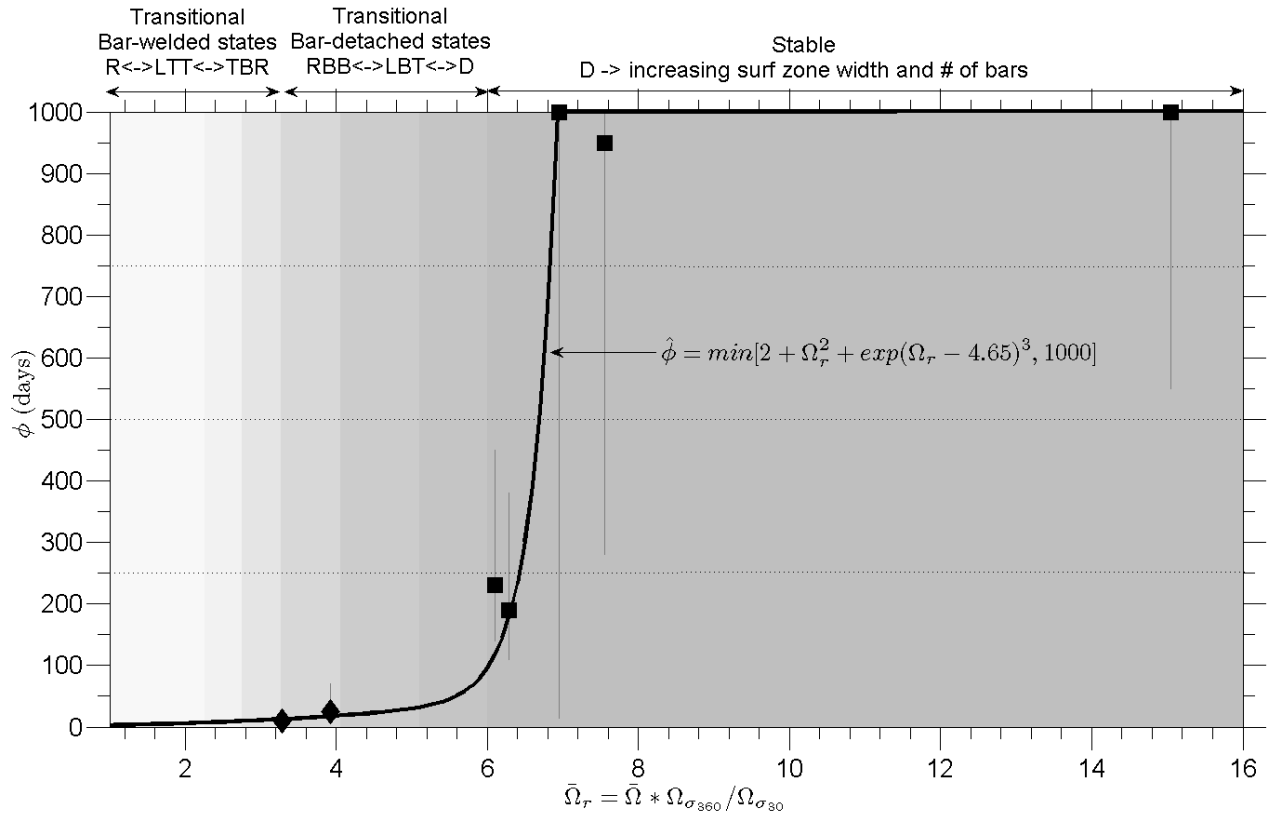


**Figure 6.** Optimized values of the response factor ( $\phi$ ) as a function of weighted dimensionless fall velocity ( $\bar{\Omega}_r$ ). Exposed coastlines are in solid squares, semi-embayed beaches are shown as solid diamonds. Grey vertical bars represent the range of  $\phi$  where model skill ( $R^2$ ) remained within 10% of maximum.  $R^2 = 0.99$ . A best-fit parameterization of the response factor ( $\hat{\phi}$ , solid line) as described in (13) is also shown.  $\hat{\phi}$  was sensibly capped at 1000 days to limit past data requirements, while not impacting the filtered  $\Omega$  time series ( $\Omega_{eq}$ ).

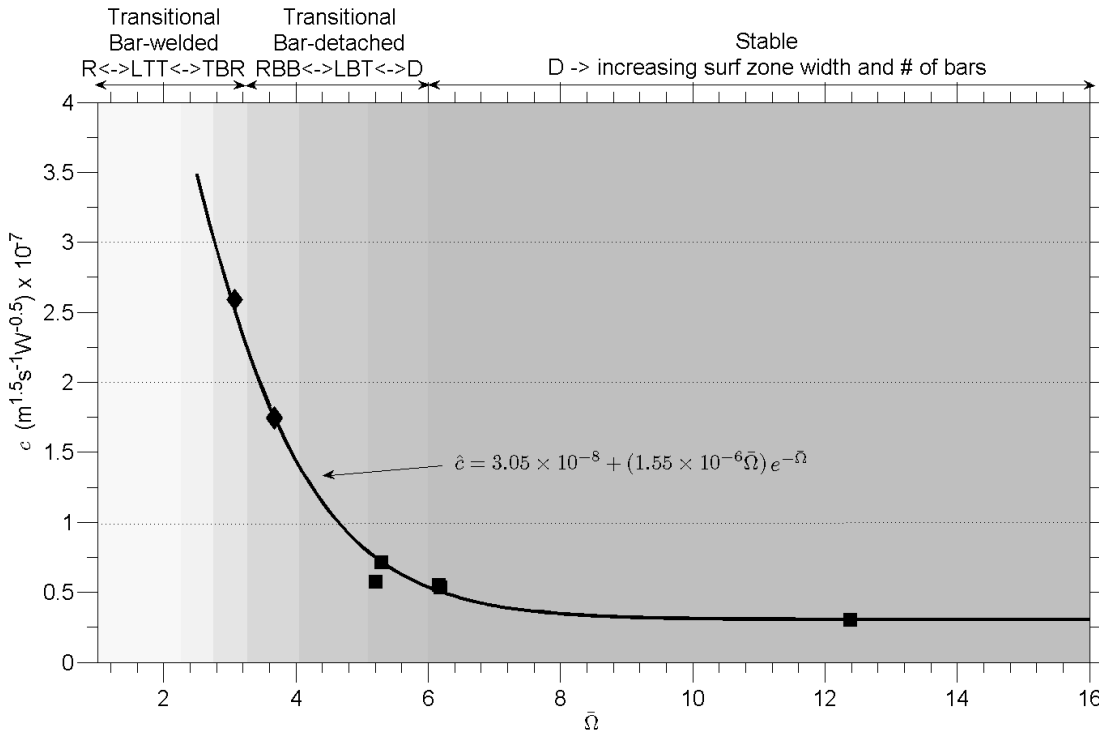


**Figure 7.** Optimized values of the rate parameter ( $c$ ) as a function of mean dimensionless fall velocity ( $\bar{\Omega}$ ). Exposed coastlines are in solid squares, semi-embayed beaches are shown as solid diamonds. A best-fit parameterization of the rate parameter (denoted  $\hat{c}$ ) as described in (14) is also shown. The extension of the parameterization beyond observations for low values of  $\bar{\Omega}$  is not included as there is insufficient data.  $R^2 = 0.99$

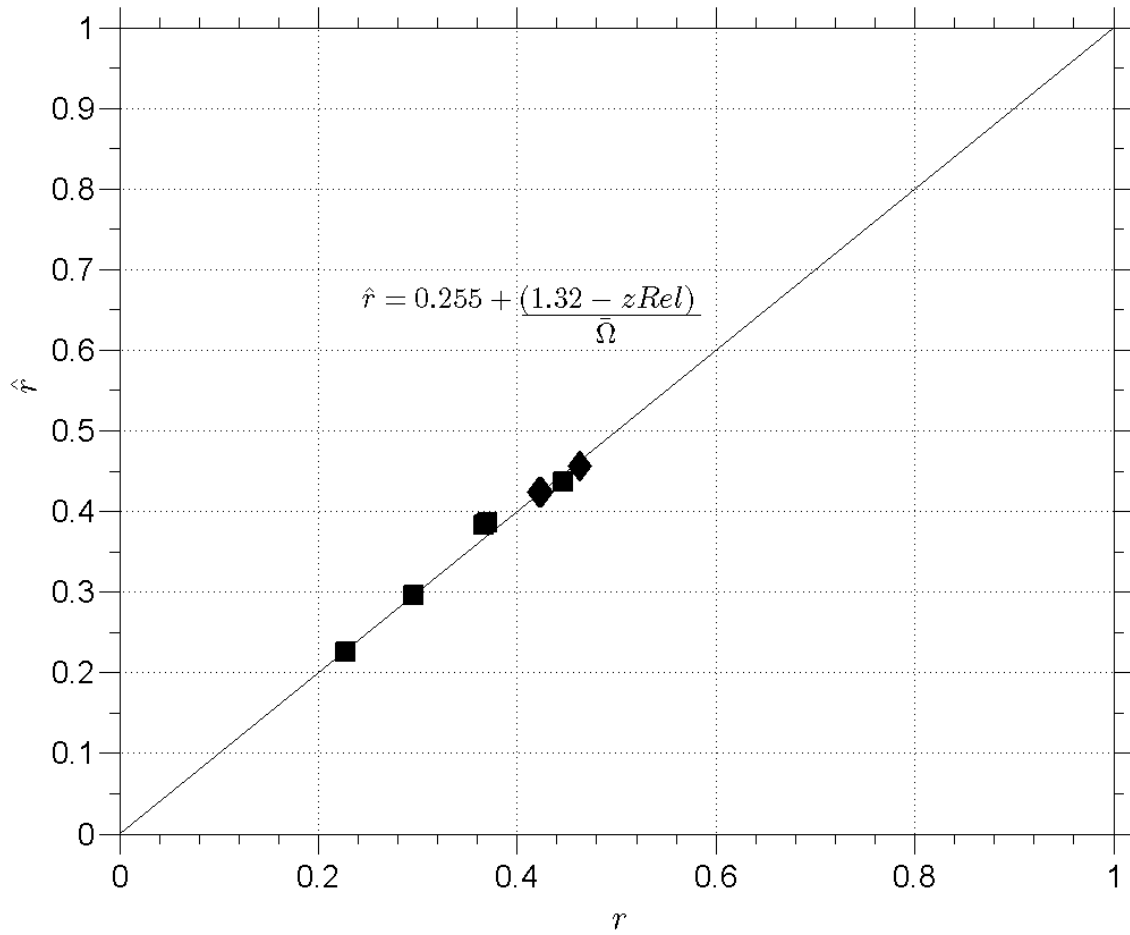


**Figure 8.** Parameterization of the erosion ratio ( $\hat{r}$ ) as a function of shoreline contour elevation with respect to MSL ( $zRel$ ) and mean dimensionless fall velocity ( $\bar{\Omega}$ ) as described in (15).  $R^2 = 0.99$ . Exposed coastlines are in solid squares, semi-embayed beaches are shown as solid diamonds.



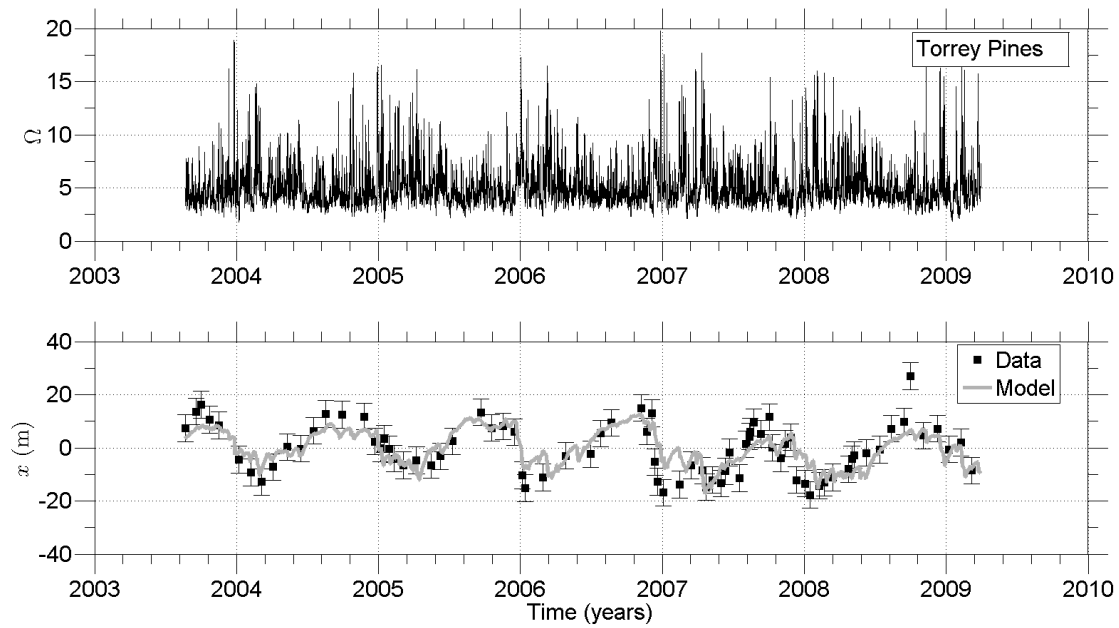


**Figure 9.** Model results for Torrey Pines utilizing the parameterizations for the response factor ( $\hat{\phi}$ , eq. 13) and the rate parameter ( $\hat{c}$ , eq. 14). Model skill was ranked as ‘good’ to ‘excellent’:  $R = 0.80$ ,  $BSS = 0.85$ ,  $NMSE = 0.37$ .